

# รายงานวิจัยฉบับสมบูรณ์

โครงการ การสังเคราะห์พอลิเมอร์บรัชที่มีสมบัติเข้ากันได้ทาง ชีวภาพโดยการริเริ่มปฏิกิริยาพอลิเมอไรเซชันจากพื้นผิว

โดย วิภาวี โฮเว่น และคณะ

เมษายน 2548

# รายงานวิจัยฉบับสมบูรณ์

# โครงการ การสังเคราะห์พอลิเมอร์บรัชที่มีสมบัติเข้ากันได้ทาง ชีวภาพโดยการริเริ่มปฏิกิริยาพอลิเมอไรเซชันจากพื้นผิว

## คณะผู้วิจัย

1. ผู้ช่วยศาสตราจารย์ ดร. วิภาวี โฮเว่น

2. ศาสตราจารย์ ดร. สุดา เกียรติกำจรวงศ์

3. นางสาวปียวรรณ สุขอินทร์

3. นางสาวมยุรี ศรีนันทากุล

### สังกัด

ภาควิชาเคมี คณะวิทยาศาสตร์
จุฬาลงกรณ์มหาวิทยาลัย
ภาควิชาวิทยาศาสตร์ทางภาพถ่ายและเทคโนโลยี
ทางการพิมพ์ คณะวิทยาศาสตร์
จุฬาลงกรณ์มหาวิทยาลัย
สาขาปิโตรเคมีและวิทยาศาสตร์พอลิเมอร์

คณะวิทยาศาสตร์ จุฬาลงกรณ์มหาวิทยาลัย สาขาปิโดรเคมีและวิทยาศาสตร์พอลิเมอร์ คณะวิทยาศาสตร์ จุฬาลงกรณ์มหาวิทยาลัย

# สนับสนุนโดยสำนักงานกองทุนสนับสนุนการวิจัย

(ความเห็นในรายงานนี้เป็นของผู้วิจัย สกว. ไม่จำเป็นต้องเห็นด้วยเสมอไป)

### **ACKNOWLEDGEMENT**

The authors would like to acknowledge Prof. Dr. Kazuhiko Ishihara for his support in MPC monomer, Assist. Prof. Dr. Junji Watanabe for GPC analysis, and most importantly Assoc. Prof. Yasuhiko Iwasaki for his support in materials, XPS and some GPC analyses as well as fruitful suggestions on solving research problems.

Special thanks go to Electronic Research Center, Faculty of Engineering, King Mongkut's Institute of Technology, Ladkrabang for ellipsometric facility; Department of Imaging and Printing Technology, Faculty of Science, Chulalongkom University and Dr. Katanchalee Mai-ngarm, National Metal and Materials Technology Center (MTEC) for providing facilities for contact angle measurements, and Capability Building Unit in Nanoscience and Nanotechnology, Department of Physics, Faculty of Science, Mahidol University for AFM facility. Financial support from the Thailand Research Fund, Teaching Assistant (TA) Fund from Chulalongkorn University and Research Assistance (RA) Fund from Organic Synthesis Research Unit (OSRU) are gratefully acknowledged.

## บทคัดย่อ

รหัสโครงการ

TRG4580049

ชื่อโครงการ

การสังเคราะห์พอลิเมอร์บรัชที่มีสมบัติเข้ากันได้ทางชีวภาพโดยการริเริ่มปฏิกิริยาพอลิเมอไรเชชัน

จากพื้นผิว

ชื่อนักวิจัย

1. ผู้ช่วยศาสตราจารย์ ดร. วิภาวี โฮเว่น

ภวควิชาเคมี คณะวิทยาศาสตร์

จุหาลงกรณ์มหาวิทยาลัย

2. ศาสตราจารย์ ดร. สูตา เกียรติกำจรวงศ์

ภาควิชาวิทยาศาสตร์ทางภาพถ่ายและเทคโนโลยี

ทางการพิมพ์ คณะวิทยาศาสตร์

จหาลงกรณ์มหาวิทยาลัย

3. นางสาวปิยวรรณ สุขอินทร์

สาขาปิโตรเคมีและวิทยาศาสตร์พอลิเมอร์

คณะวิทยาศาสตร์ จุฬาลงกรณ์มหาวิทยาลัย

4. นางสาวมยุรี ศรีนั้นทากุล

สาขาปิโตรเคมีและวิทยาศาสตร์พอลิเมอร์

คณะวิทยาศาสตร์ จุฬาลงกรณ์มหาวิทยาลัย

E-mail Address :

vipavee.p@chula.ac.th

ระยะเวลาโครงการ :

1 กรกฎาคม 2545 - 30 มิถุนายน 2547

พอลิเมอร์บรัชที่มีความเข้ากันได้ทางชีวภาพสามารถเตรียมได้จากปฏิกิริยาพอลิเมอไรเซซันที่ริเริ่มจากพื้นผิวโดยผ่าน กลไกแบบอะดอมทรานส์เพ่อร์เรดิคัลพอลิเมอไรเซชันของ 2-เมทอะคริโลอิลออกชิเอทิลฟอสพ่อริลโคลีน (เอ็มพีซี) จาก พื้นผิวที่ยึดติดด้วยหมู่ริเริ่มที่ประกอบด้วยแอลฟาโบรโมไอโซบิวทีเรต โดยมีคอปเปอร์โบรไมด์และไบไพริคิลเป็นระบบ เร่งปฏิกิริยา ความสัมพันธ์แบบเส้นตรงระหว่างน้ำหนักโมเลกุลและความหนากับเวลาแสดงให้เห็นว่าปฏิกิริยาพอลิเมอ ไรเชชันมีกลไกเป็นอมตะ โดยได้ความหนาแน่นการกราฟต์ 0.3-0.5 สายใช่/ตารางนาโนเมตร สามารถใช้โมเลกุลชั้น เดียวของทริสไทรเมทิลใชลอกชีไชลิล (ทริสทีเอ็มเอส) เป็นแม่แบบระดับนาโนเมตรในการควบคุมความหนาแน่นการ กราฟต์ของพีเอ็มพีซีบรัช ส่วนที่อื่นนูนซึ่งสังเกตเห็นได้จากภาพเอเอฟเอ็มของพีเอ็มพีซีบรัชเป็นหลักฐานที่แสดงให้ เห็นว่าพีเอ็มพีซีบรัชมีการกระจายตัวในระดับนาโนเมตรบนชับสเทรต ขนาดของส่วนที่ยื่นนูนและความขรุขระของ พื้นผิวมีลักษณะลอดคล้องเป็นอย่างดีกับความหนาแน่นการกราฟด์ของพีเอ็มพีซีบรัช นอกจากนี้ยังพิสูจน์ได้ว่าการจับ ้ตัวกันเองเป็นกลุ่มก้อนของพีเอ็มพีซึบรัชเกิดจากการเข้ากันไม่ได้ระหว่างเฟสของพีเอ็มพีซีบรัชที่มีสมบัติชอบน้ำและ หมู่ทริสทีเอ็มเอสที่มีสมบัติไม่ชอบน้ำ ผลจากการวิเคราะห์การดูดซับของโปรตีนและการยึดเกาะของเกล็ดเลือดแสดงให้ เห็นว่าพีเอ็มพีซีบรัชที่มีการกราฟต์อย่างหนาแน่นและทั่วถึงมีสมบัติเข้ากันได้กับเลือด ส่วนในกรณีที่พีเอ็มพีซีบรัช เติบโหจากรูขนาดนาโนแบบไม่หนาแน่นและไม่ทั่วถึงนั้น การดูดชับของโปรตีนขึ้นกับร้อยละการปกคลุมของทริสทีเอ็ม เอสเมื่อใช่ของพอลิเมอร์บรัชค่อนข้างสั้นเท่านั้น จากความจริงที่ว่าไม่มีความสัมพันธ์อย่างจำเพาะเจาะจงระหว่างร้อย ละการบ่าคลุมของหริสทีเอ็มเอสกับการยึดเกาะของเกล็ดเลือดแสดงให้เห็นว่าการกระจายของพีเอ็มพีซีบรัชระดับนาโน เมตรมีขนาดเล็กเกินกว่าที่เกล็ดเลือดที่มีขนาดระดับไมครอนจะตระหนักถึงความต่างเนื้อของพื้นผิว

คำหลัก : เอทีอาร์พี พอลิเมอร์บรัช แม่แบบสเกลนาโน เอ็มพีซี ปฏิกิริยาพอลิเมอไรเซชันริเริ่มจากพื้นผิว

### **ABSTRACT**

Project Code TRG4580049

Project Title Synthesis of Biocompatible Polymer Brush by Surface-initiated Polymerization

Investigator

Assist, Prof. Vipavee P. Hoven, Ph.D. Department of Chemistry, Faculty of Science

Chulalongkorn University

2. Prof. Suda Kiatkamjornwong, Ph.D. Department of Photoimaging and Printing

Faculty of Science, Chulalongkorn University

Miss Piyawan Suk-in Program of Petrochemistry and Polymer Science,

Faculty of Science, Chulalongkorn University

Miss Mayuree Srinanthakul Program of Petrochemistry and Polymer Science,

Faculty of Science, Chulalongkorn University

E-mail Address: vipavee.p@chula.ac.th

Project Period : July 1, 2002 - June 30, 2004

Preparation of biocompatible polymer brush was accomplished by surface-initiated atom transfer radical polymerization of 2-methacryloyloxyethyl phosphorylcholine (MPC) from surface-tethered α-bromoisobutyrate using CuBr/bpy as a catalytic system. The linear dependence of molecular weight and thickness on polymerization time clearly suggested that polymerization is fiving. The graft density of 0.3-0.5 chains/nm<sup>2</sup> was achieved. Chemically grafted tris(trimethylsiloxy)silyl (tris(TMS)) monolayer can be used as a nanometerscale template for controlling the graft density of PMPC brushes. Protrusions observed from AFM images of PMPC brushes evidently suggested that PMPC brushes distributed nanoscopically on the substrate. The size of protrusion and surface roughness corresponded quite well with the graft density of PMPC brushes. The self-aggregation of PMPC brushes in nanopores was proven to be a consequence of phase incompatibility between hydrophilic PMPC brushes and hydrophobic tris(TMS). As evaluated by protein adsorption and platelet adhesion studies, homogeneously and densely grafted PMPC brushes are apparently blood compatible. In the case of heterogeneously and loosely grafted PMPC brushes grown from nanopores, the protein adsorption was varied as a function of %tris(TMS) coverage only when polymer brushes were relatively short in length. The fact that there was no specific correlation between %tris(TMS) and platelet adhesion implied that the distribution of PMPC brushes in nanometer scale was definitely too small for the micron-sized platelets to recognize the heterogeneity of surface.

Keywords: ATRP, polymer brush, nano-scale template, MPC, surface-initiated polymerization

## **CONTENTS**

		Page
ACKNOWLEDG	EMENT	i
ABSTRACT IN	THAI	íi
AB\$TRACT IN	ENGLISH	iii
LIST OF FIGUR	RES	vi
LIST OF TABLE	S	×
LIST OF SCHE	MES	xì
CHAPTER I : IN	NTRODUCTION	1
1.	1 Significance of Research Problem	1
1.	2 Objectives	3
CHAPTER # : T	THEORY AND LITERATURE REVIEW	4
2.	1 Development of Phosphorylcholine-containing	
	Momomer	4
2.	2 Living Polymerization	7
2.	3 Polymer Brush	14
2.	4 Patterned Polymer Film	19
2	5 Blood Compatibility	23
2.	6 Characterization Techniques	26
CHAPTER III :	EXPERIMENTAL	33
3.	1 Materials	33
3.	2 Equipments	34
3	3 Procedures	36
3.	.4 Protocol for Blood Compatibility Test	43
CHAPTER IV :	RESULTS AND DISCUSSION	45
4	.1 Synthesis of α-Bromoester Derivatives to be used as	
	Initiators	45
4	.2 Preparation of Silicon -supported Mixed Tris(TMS)/silanol	
	Monolayer	52

4.3	Preparation of Silicon-supported α-Bromoisobutyrate	
•	Monolayer	56
4.4	Preparation of Silicon-supported Mixed Tris(TMS)/α-	
	Bromoisobutyrate Monolayer	58
4.5	Surface-initiated Polymerization of MPC from Silicon-	
	supported α-Bromoisobutyrate Monolayer	60
4.6	Surface-initiated Polymerization of MPC from Silicon-	
	supported Mixed Tris(TMS)/α-Bromoisobutyrate Monolayer	72
4.7	Surface Topography of PMPC Brushes	77
4.8	Biocompatibility of PMPC Brushes	85
CHAPTER V : EXE	ECUTIVE SUMMARY	90
REFERENCES		92
OUTPUT		102
APPENDIX		103

## LIST OF FIGURES

Figure		Page
2.1	Molecular weight conversion curves for various kinds of	
	polymerization methods: (A) living polymerization; (B) free radical	
	polymerization; and (C) condensation polymerization	9
2.2	Architectural forms of polymers available by living polymerization	
	techniques	10
2.3	Examples of polymer systems comprising polymer brushes	16
2.4	Classification of linear polymer brushes, (a <sub>1</sub> -a <sub>4</sub> ) homopolymer brushes;	
	(b) mixed homopolymer brush; (c) random copolymer brush; (d) block	
	copolymer brush	18
2.5	Preparation of polymer brushes by "physisorption", "grafting to" and	
	"grafting from"	18
2.6	Strategy for amplification of a patterned SAM prepared by $\mu$ CP into a	
	patterned polymer brush	21
2.7	AFM images (height/phase) of 11K PS-COOH adsorbed from toluene to	
	tris(TMS) -modified surfaces	23
2.8	Pictorial representation of human blood	24
2.9	Schematic representation of blood coagulation system	25
2.10	Schematic of the geometry of an ellipsometry experiment	26
2.11	Schematic representation of the Young's equation	27
2.12	Schematic representation of wettability	27
2.13	Schematic diagram of the X-ray photoelectron emission process	28
2.14	General schematic drawing of the XPS instrument	29
2.15	Schematic diagram of an atomic force microscope	32
4.1	<sup>1</sup> H NMR spectra of (A) prop-2-enyl-2-bromoisobutyrate and (B) 3-	
	(dimethylethoxysilyl)propyi-2-bromoisobutyrate	49
4.2	<sup>1</sup> H NMR spectra of (A) hex-5-enyl-2-bromoisobutyrate and (B) 6-	
	(dimethylethoxysilyl)hexyl-2-bromoisobutyrate	50
4.3	<sup>1</sup> H NMR spectra of (A) dec-9-enyl-2-bromoisobutyrate and (B) 10-	
	(dimethylethoxysilyl)decyl-2-bromoisobutyrate	51

# LIST OF FIGURES (Continued)

Figure		Page
4.4	<sup>1</sup> H NMR spectrum of propyl-2-bromoisobutyrate	52
4.5	Ellipsometric thickness of tris(TMS) monolayer as a function of reaction	
	time	53
4.6	Water contact angle of tris(TMS) monolayer as a function of reaction	
	time: advancing angle (●) and receding angle (○)	54
4.7	Schematic representation of nanopores in tris(TMS) monolayer	56
4.8	Advancing (O) and receding (  ) water contact angle data of silicon	
	oxide surface after a reaction with 4 as a function of reaction time	57
4.9	Ellipsometric thickness of the surface grafted $lpha$ -bromoester initiator as	
	a function of reaction time	57
4.10	<sup>1</sup> H NMR spectra of (a) MPC and (b) PMPC mixed with the unreacted	
	MPC synthesized by ATRP using [OEGBr]:[MPC] = 1:20	60
4.11	%Monomer conversion as a function of reaction time using water (O),	
	methanol:water = 1:1 (v/v) (●), and 4:1 (v/v) (□) as a solvent	62
4.12	Ellipsometric thickness of PMPC brushes versus polymerization time in	
	the presence of "added" initiator, [MPC]:[added initiator] = 200:1 (O)	
	and [MPC]:[added initiator] = 50:1(●) using methanol:water = 4 :1 (v/v)	
	as a solvent	64
4.13	Ellipsometric thickness of PMPC brushes versus polymerization time for	
	targeted DP = 200 in methanol:water = 4:1 (v/v) (■) and pure methanol	
	(🗆)	65
4.14	Water contact angle data of PMPC brushes versus polymerization time	
	for targeted DP = 200 using methanol/water = 4:1 (v/v) as a solvent: $\theta_{\text{A}}$	
	(●) and $\theta_{R}$ (○)	66
4.15	Ellipsometric thickness ( $ullet$ ) and receding water contact angle ( $eta_{\text{R}}$ ) ( $\bigcirc$ )	
	of PMPC brushes versus polymerization time for targeted DP = 200	
	using methanol:water = 4:1 (v/v) as a solvent	66
4.16	Ellipsometric thickness ( $\blacksquare$ ) and receding water contact angle ( $\theta_{\text{R}}$ ) ( $\square$ )	
	of PMPC brushes versus polymerization time for targeted DP = 200	
	using methanol as a solvent	67

# LIST OF FIGURES (Continued)

Figure		Page
4.17	Ellipsometric thickness of PMPC brushes versus polymerization time for	
	different [CuBr]/[CuBr2] ratios at targeted DP of 200 using	
	methanol:water = 4:1 (v/v) as a solvent: [CuBr]/[CuBr₂] = 1:0 (●), 1:0.1	
	(□) and 1:0.5 (▲)	68
4.18	Molecular weight $(\overline{M}_{ m n})$ ( $ullet$ ) and molecular weight distribution	
	$(\overline{M}_{w}/\overline{M}_{n})$ (O) of free PMPC for targeted DP = 200 produced in	
	methanol:water = 4:1 (v/v) as a function of polymerization time	69
4.19	Relationship between ellipsometric thickness of PMPC brushes and	
	molecular weight ( $\overline{M}_{ m n}$ ) of free PMPC for targeted DP = 200 produced	
	in methanol:water = 4:1 (v/v)	70
4.20	Relationship between ellipsometric thickness of PMPC brushes and	
	molecular weight ( $\overline{M}_{ m n}$ ) of free PMPC for targeted DP = 50 produced in	
	methanol:water = 4:1 (v/v)	70
4.21	Ellipsometric thickness of PMPC brushes grown from silicon-supported	
	mixed tris(TMS)/α-bromoisobutyrate monolayer using methanol (●) or	
	water (O) as a solvent	73
4.22	Water contact angle of PMPC brushes grown from silicon-supported	
	mixed tris(TMS)/α-bromoisobutyrate monolayer using methanol as a	
	solvent for 5 h: $ heta_{A}$ ( $ullet$ ) and $ heta_{R}$ (O)	74
4.23	Ellipsometric thickness (●) and receding water contact angle (O) of	
	silicon-supported mixed tris(TMS)/PMPC brushes having 82% tris(TMS)	
	coverage as a function of polymerization time	77
4.24	Ellipsometric thickness of PMPC brushes grown from silicon-supported	
	mixed tris(TMS)/Q-bromoisobutyrate monolayer having 82% tris(TMS)	
	coverage versus grafting time of initiator in methanol for 5 h: n₃ (●), n₀	
	(O)and n <sub>10</sub> (▲)	76
4.25	Ellipsometric thickness of PMPC brushes grown from silicon-supported	
	mixed tris(TMS)/∝-bromoisobutyrate monolayer having 82%tris(TMS)	
	coverage versus polymerization time in methanol : n <sub>3</sub> (•), n <sub>6</sub> (O)and n <sub>10</sub>	
	(📤)	77

# LIST OF FIGURES (Continued)

Figure		Page
4.26	AFM images of silicon-supported mixed tris(TMS)/silanol monolayer	
	having varied %tris(TMS) coverage: (a) 0%, (b) 51%, (c) 66%, and (d)	
	82% and silicon-supported mixed tris(TMS)/Q-bromoisobutyrate	
	monolayer having varied %tris(TMS) coverage: (e) 0%, (f) 51%, (g)	
	66%, and (h) 82%	78
4.27	AFM images of silicon-supported mixed tris(TMS)/PMPC brushes	
	prepared in methanol for 1 h having varied %tris(TMS) coverage : (a)	
	0%, (b) 51%, (c) 66% and (d) 82%	80
4.28	AFM images of silicon-supported mixed tris(TMS)/PMPC brushes having	
	82% tris(TMS) coverage prepared in methanol for 1 h by controlling	
	grafting time of initiator: (a) 1 day, (b) 2 days, (c) 3 days and (d) 4 days	82
4.29	Schematic representation of possible orientation of polymer brushes	
	grown from nanopores having different graft density	82
4.30	AFM images of silicon-supported mixed tris(TMS)/PMPC brushes	
	prepared in methanol for 1 h using grafting time of initiator for 1 day	
	and having varied % tris(TMS) coverage: (a) 0%, (b) 51%, (c) 66% and	
	(d) 82%	83
4.31	AFM images of silicon-supported mixed tris(TMS)/PtBMA brushes	
	having 82% tris(TMS) coverage prepared in toluene at 90°C for 1 h by	
	controlling grafting time of initiator: (a) 1 day and (b) 4 days	84
4.32	AFM images of silicon-supported mixed tris(TMS)/PtBMA brushes	
	having 82% tris(TMS) coverage prepared in toluene at 90 °C for 5 h by	
	controlling grafting time of initiator: (a) 1 day and (b) 4 days	85
4.33	Calibration curve of the amount of albumin adsorbed and the	
	absorbance obtained from BCA microassay	86
4.34	SEM micrographs of various silicon surfaces after contacting with	
	human PRP	89

## LIST OF TABLES

Table		Page
4.1	Characteristic $^1$ H NMR peaks and %yield of vinyl-terminated $lpha$ -	46
	bromoisobutyrate compounds	
4.2	Characteristic <sup>1</sup> H NMR peaks and %yield of silane compounds	48
4.3	XPS data (15° take-off angle), water contact angle and calculated %	
	coverage of tris(TMS) monolayer as a function of reaction time	55
4.4	XPS atomic composition (15° takeoff angle) and contact angle data for	
	silicon-supported mixed tris(TMS)/∞-bromoisobutyrate (n=3) monolayer	
	using 4 days of reaction	59
4.5	XPS elemental surface composition (%) of silicon surfaces before and	
	after the formation of PMPC brushes	72
4.6	Average roughness of silicon-supported mixed surfaces determined by	
	AFM analysis	79
4.7	Average roughness (Ra) of silicon-supported mixed tris(TMS)/PMPC	
	brushes prepared in methanol determined by AFM analysis	81
4.8	The amount of plasma protein adsorbed on various silicon substrates	87

## LIST OF SCHEMES

Scheme		Page
2.1	Synthetic route of MPC: (a) Nakabayashi et al. [5]; (b) Ishihara et	
	al	5
2.2	Synthetic route of MPCE	7
2.3	Mechanism of ATRP	11
2.4	Equilibrium reaction in ATRP	11
2.5	Rotation of bpy ligand from the tetrahedral to penta-coordinated species	
	when alkyl bromide is incorporated	12
2.6	Complex formation equilibrium in polar and nonpolar solvents	13
4.1	Mechanism of hydrosilylation using chloroplatinic acid as a catalyst	48
4.2	The activation/deactivation cycles of ATRP process	63

### CHAPTER I

### INTRODUCTION

#### 1.1 Significance of Research Problem

The control of surface property is of crucial significance in many areas of modern science and technology ranging from biotechnology to advanced microelectronics. Surfacetethered polymer brush is considered as one of novel approaches for surface modification. Conventionally, polymer brushes are prepared by adsorption of block copolymers where one block is strongly adsorbed to the surface with the other block forming the brush layer. The noncovalent nature of this grafting strategy is a weakness, however, since the desorption of the brush can subsequently occur. In addition, the demanding block copolymer synthesis limits the choice of functional groups for the block copolymer structure. Another method is to use the "grafting to" technique, in which preformed polymer chains in solution are tethered to the surface. This method does not allow high-density brushes to be formed due to the exclusion of chains as the graft density grows. Nonetheless, the molecular weight distribution can be easily controlled since polymer fractions with narrow molecular weight can be used. The other approach, in principle more versatile, is the "grafting form" or the "surface-initiated polymerization" technique, in which polymerization is initiated from initiators coupled covalently to the surface. One should be able to grow very high-density polymer brushes on a substrate using the latter method, if proper conditions are employed.

The use of controlled/living polymerization for surface-initiated polymerization should be optimal because such methods afford good control over the molecular weight, molecular weight distribution, and structure of the resulting polymer. Several mechanisms have been used to grow polymer chains from a surface, including radical, anionic, cationic, ring-opening, ring-opening metathesis. There is growing interest in atom transfer radical polymerization (ATRP) since it was discovered in 1995. The living characteristic and the compatibility with a variety of functional monomer render ATRP an attractive method for surface-initiated polymerization in producing well-defined polymer brushes. The success of ATRP in synthesizing hydrophilic polymers provides an additional advantage over the traditional living ionic polymerization.

There has been considerable amount of research work reported on the micromanipulation of protein adsorption and cell adhesion on solid surfaces. The development of biosensors and drug screening arrays are among potential applications of such research. It is generally difficult to control protein adsorption and corresponding cell adhesion because nonspecific protein adsorption is the first phenomenon when the surface comes in contact with physiological environment. Non-fouling or protein-resistant properties are thus important in the control of protein adsorption and cell adhesion.

As inspired by the biomembrane-like structure, a methacrylate monomer bearing a polar phospholipid group, 2-methacryloyloxyethyl phosphorylcholine (MPC) was developed. The MPC polymers exhibit a property that resists nonspecific interaction with plasma proteins and cells. The excellent non-fouling property of the MPC polymers is proven to originate from the ability to induce self-assembly of natural phospholipids. It has also been shown that the activation and inflammatory response of cells in contact with MPC polymers are not induced. Since hydrophilic MPC homopolymer possesses inferior mechanical properties, MPC is generally used in the form of copolymers, polymer coating and grafting. Despite the success of MPC polymers as biomimetic polymers having biocompatible and non-fouling characteristics, the effects of their surface structures at microscopic and nanoscopic level in responses to protein and cells have not yet been explored.

To produce surfaces tethered with well-defined MPC polymers or PMPC brushes, surface-initiated polymerization using ATRP undoubtedly appear as a primary choice. The study is also challenging from the fact that very few ATRP trials to optimize protein/material or cell/material interface, that is biointerface, have been reported. The issue related to the formation of PMPC brushes with well-defined thickness and graft density is a subject of our interest. The thickness of PMPC brushes is controlled by experimental parameters such as polymerization time, monomer to initiator ratio.

From both theoretical and practical perspectives, several aspects related to the graft density of polymer brushes and surface properties are very important. In principle, the graft density of polymer brushes depends upon the density of grafted initiator on a substrate surface. In this research, chemically grafted tris(trimethylsiloxy)sityl (tris(TMS)) monolayer is used as a nanometer-scaled template for controlling the graft density of PMPC brushes. By controlling the kinetic of a reaction between silanol groups on the silicon oxide surface with tris(trimethylsiloxy) chlorosilane (tris(TMSCI), surfaces having a range of tris(TMS) coverage can be generated.

The incomplete reaction between the sluggish tris(TMSCI) and silicon oxide surface allows a mixed tris(TMS)/silanol surface to be formed. α-bromoester groups can be subsequently attached to the residual silanol groups in nanopores of the substrate. Polymer brushes of 2-methacryloyloxyethyl phosphorylcholine (MPC) are then prepared by surface-initiated ATRP from nanoporous surface. The correlation between the graft density of polymer brushes and surface topography is also explored.

Since MPC polymers are recognized to resist protein adsorption, biocompatibility of PMPC brushes, in this particular study, is addressed in terms of responses to plasma components namely proteins and platelets. We anticipate that PMPC brushes with controlled thickness and graft density would allow a better control of biological responses at microscopic or nanoscopic level of the material's surface.

#### 1.2 Objectives

- To synthesize poly(2-methacryloyloxyethyl phosphorylcholine) brushes by surfaceinitiated atom transfer radical polymerization
- 2. To study the effect of thickness and graft density of poly(2-methacryloyloxyethyl phosphorylcholine) brushes on plasma protein adsorption and platelet adhesion
- To study the correlation between graft density and surface topography of poly(2methacryloyloxyethyl phosphorylcholine) brushes

### **CHAPTER II**

### THEORY AND LITERATURE REVIEW

#### 2.1 Development of Phosphorylcholine-containing Monomer

A biomembrane is a hybrid that consists of two chemical units, phospholipids and proteins. There is no covalent bonding between these, thus, the surface of a biomembrane is heterogeneous and dynamic. New biomaterials were proposed whose activity is based upon the mimicking of a simple component present on the extracellular surfaces of the phospholipid bilayer that forms the matrix of the cell membranes of blood cells, namely, the phosphorylcholine group of phosphatidylcholine and sphingomyelin. Phosphorylcholine, an electrically neutral, zwitterionic headgroup, is one of the phospholipid headgroups existing on the external surface of blood cells, and it is inert in coagulation assays. The blood compatibility of a polymer surface coated with phospholipids was confirmed by several researchers [1-2]. For example, the interactions between polyamide microcapsules coated with the phospholipid-bilayer membrane and platelets were investigated [2]. It was found that platelet adhesion onto the microcapsules was significantly suppressed by the phospholipid coating. The mobility of the phospholipid layer coated on the surface affected the platelet adhesion. When the phospholipids were in a liquid crystalline state, platelet adhesion was smaller than that observed when the phospholipids on the surface were in a gel state [3].

New concepts for making blood-compatible polymeric materials that utilize the characteristics of natural phospholipid molecules in plasma have been proposed [4]. It was thought that if a polymer surface possesses a phospholipid-like structure, a significant amount of natural phospholipids in plasma could be adsorbed onto the surface through self-assembly [4]. Based on this idea, a methacrylate monomer with a phospholipid polar group, 2-methacryloyloxyethyl phosphorylcholine (MPC) was designed and synthesized [5-6] (Scheme 2.1). The excellent blood compatibility of the MPC-containing materials is proven to originate from the capability to induce self-assembly of natural phospholipids.

Scheme 2.1 Synthetic route of MPC: (a) Nakabayashi et al. [5]; (b) Ishihara et al. [6]

In 2001, Hasegawa's group prepared polymer blends composed of polysulfone and 2-methacryloyloxyethyl phosphorylcholine (MPC) polymer (PSf/MPC polymer) to obtain protein-resistant membrane for hemodialysis. The content of the MPC polymer in the blends was 7 and 15 wt%. The asymmetric porous membrane was obtained by dry/wet membrane processing method. The mechanical strength of the PSf/MPC polymer membrane did not change compared with that of the PSf membrane. On the other hand, the permeability of solute having molecular weight below 2.0 x 10<sup>4</sup> through the PSf membrane increased with the addition of the MPC polymer, which is considered to be an effect of the hydrophilic character of the MPC polymer. The amount of protein adsorbed on the PSf membrane from plasma was reduced by the addition of the MPC polymer. Platelet adhesion was also effectively suppressed on the PSf/MPC polymer membrane. Based on these results, the MPC polymer could serve as a doubly functional polymeric additive, that is, to generate a protein-resistant characteristic and to render the membrane hydrophilic [7]: In the same year, Konno and coworkers prepared the poly(L-lactic acid) nanoparticles immobilized with MPC polymer, which has excellent blood compatibility by a solvent evaporation technique using the water-soluble amphiphilic MPC polymer as an emulsifier and a surface modifier. The diameter and C-potential of the obtained nanoparticles strongly depended on the concentration of the MPC polymer. Furthermore, various hydrophobic fluorescence probes could permeate through the MPC polymer layer and adsorb on the PLA surface. The amount of bovine serum albumin adsorbed on the nanoparticles was significantly smaller compared with that on the conventional polystyrene nanoparticles [8].

In 2002, new segmented polyurethanes (SPUs) grafted with phospholipid analogous vinyl monomer, 2-methacryloyloxyethyl phosphorylcholine (MPC) on surface were synthesized by Korematsu and coworkers. They found that fewer platelets adhered to the MPC-grafted surfaces [9]. In the same year, Uchiyama and coworkers prepared a novel polymer alloy membrane with both biocompatibility and permeability for fabrication of an implantable artificial pancreas. The polymer alloy was composed of a segmented (SPU) and a phospholipid polymer with 2-methacryloyloxyethyl phosphorylcholine (MPC) units. The MPC polymer was poly(MPC-co-2-ethylhexyl methacrylate) (PMEH), which can be dissolved in the same solvent for SPU. The SPU/PMEH alloy membrane was prepared by a solvent evaporation method. They found that the SPU/PMEH alloy membrane had excellent mechanical properties. The glucose and insulin could permeate through the SPU/PMEH alloy membrane. The reduction of the number of fibroblasts that adhered to the surface of the SPU/PMEH alloy membrane was observed. That is, it has a good biocompatible surface compared with the original SPU. It was suggested that excellent functions, such as good insulin permeability, and reduction of fibroblast adhesion were promoted by the PMEH which dispersed both on the surface and inside the membrane [10].

In 2003, Yamasaki and coworkers studied the effects of the surface properties of phospholipid polymers having various bridging units between the phosphorylcholine and the backbone on their blood compatibility. The copolymers between 2-methacryloyloxyethyl phosphorylcholine (MPC), 2-methacryloyloxy ethoxyethyl phosphorylcholine (MEO2PC), and 6-methacryloyloxyethoxyhexyl phosphorylcholine (MHPC) with n-butyl methacrylate (BMA) were prepared. It was found that the surface density of adsorbed proteins and adherent platelets on the poly(MPC-co-BMA) was similar to that on poly(BMA). On the other hand, poly(MEO2PC-co-BMA) and poly(MHPC-co-BMA) effectively reduced biofouling compared with poly(MPC-co-BMA). They clarified that the copolymer surfaces having long bridging units, which could easily form a phosphorylcholine-enriched surface when the blood was in contact with the surface, showed excellent blood compatibility without prehydration [11]. Furthermore, in the same year, Zhu and coworkers synthesized 2-methacryloyloxyethyl phosphorylcholine (MPCE) using phosphorous trichloride, ethylene glycol, 2-hydroxyethyl

methacrylate (HEMA) and triethylamine (Scheme 2.2), and then used in the preparation of O-butyrylchitosan-bonded MPCE (MPCE-BCS) by Michael addition of MPCE to amino groups of O-butyrylchitosan. The blood-compatibility of MPCE-BCS was evaluated by means of blood clotting and platelet adhesion assays. The blood-clotting assay indicated that O-butyrylchitosan was haemo-compatible. Both the blood-clotting assay and platelet adhesion assay confirmed that MPCE-BCS had excellent antithrombogenicity [12].

PCI<sub>3</sub> + HOCH<sub>2</sub>CH<sub>2</sub>OH 
$$\bigcirc$$
  $\bigcirc$  P-CI  $\bigcirc$   $\bigcirc$  P-CI  $\bigcirc$   $\bigcirc$  P-CI  $\bigcirc$   $\bigcirc$  P-CI  $\bigcirc$  P-CI  $\bigcirc$  P-CI  $\bigcirc$  P-CI  $\bigcirc$  P-CI  $\bigcirc$  P-CI  $\bigcirc$   $\bigcirc$  P-CI  $\bigcirc$ 

Scheme 2.2 Synthetic route of MPCE [12]

#### 2.2 Living Polymerization

Synthetic polymers are long-chain molecules possessing uniform repeat units (mers). The chains are not all the same length. These giant molecules are of interest because of their physical properties, in contrast to low molecular weight molecules, which are of interest due to their chemical properties. Possibly the most useful physical property of polymers is their low density versus strength.

When synthetic polymers were first introduced, they were made by free radical initiation of single vinyl monomers or by chemical condensation of small difunctional molecules. The range of their properties was understandably merger. However, polymer chemists realized that their materials could not compare with the properties of natural polymers, such as wool, silk, cotton, rubber, tendons, and spider webbing. The natural polymers are generally condensation polymers made by addition of monomer units one at a time to the ends of growing polymer chains. Polymerization of all chains stops at identical molecular weights. For some time polymer chemists have realized that to approach nature's degree of sophistication, new synthetic techniques would be needed.

Conventional chain-growth polymerizations, for example, free radical synthesis, consist of four elementary steps: initiation, propagation, chain transfer, and termination. As early as 1936, Ziegler proposed that anionic polymerization of styrene and butadiene consecutive addition of monomer to an alkyl lithium initiator occured without chain transfer or termination. During transferless polymerization, the number of polymer molecules remains contant. Since there is no termination, active anionic chain ends remain after of the monomer has been polymerized. When fresh monomer is added, polymerization resumes. The name "living polymerization" was coined for the method by Szwarc [13]. Because the chain ends remain active until killed. (The term has nothing to do with living in the biological sense.) Before Szwarc's classic work, Flory [14] had described the properties associated with living polymerization of ethylene oxide initiated with alkoxides. Flory noted that since all of the chain ends grow at the same rate, the molecular weight is determined by the amount of initiator used versus monomer (Eq.1)

Another property of polymers produced by living polymerization is the very narrow molecular weight distribution. The polydispersity (D) has a Poisson distribution,  $D=\overline{M}_{\rm w}/\overline{M}_{\rm n}=1+(1/dp)$ ;  $\overline{M}_{\rm w}$  is the average molecular weight determined by light scattering,  $\overline{M}_{\rm n}$  is the average molecular weight determined by osmometry, and dp is the degree of polymerization (the number of monomer units per chain). The values of  $\overline{M}_{\rm w}$  and  $\overline{M}_{\rm n}$  can also be determined by gel permeation chromatography (GPC). A living polymerization can be distinguished from free radical polymerization or from a condensation polymerization by plotting the molecular weight of the polymer versus conversion. In a living polymerization, the molecular weight is directly proportional to conversion (Figure 2.1, line A). In a free radical or other nonliving polymerization, high molecular weight polymer is formed in the initial stages (line B), and in a condensation polymerization, high molecular weight polymer is formed only as the conversion approaches 100% (line C).

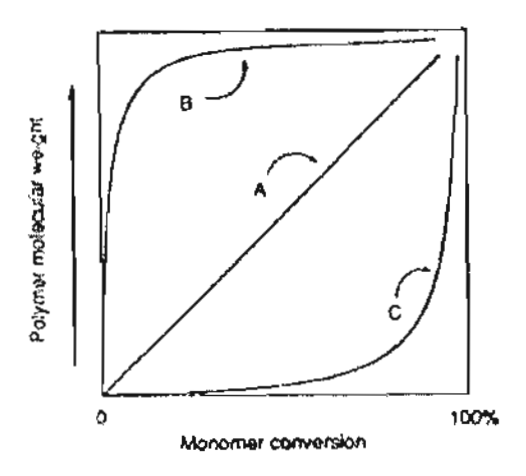


Figure 2.1 Molecular weight conversion curves for various kinds of polymerization methods:

(A) living polymerization; (B) free radical polymerization; and (C) condensation polymerization [14]

Living polymerization techniques give the synthetic chemist two particularly powerful tools for polymer chain design: the synthesis of block copolymers by sequential addition of monomers and the synthesis of functional-ended polymers by selective termination of living ends with appropriate reagents. The main architectural features available starting with these two basic themes are listed in Figure 2.2 along with applications for the various polymer types. Although living polymerization of only a few monomers is nearly perfect, a large number of other systems fit theory close enough to be useful for synthesis of the wide variety of different polymer chain structures in general, the well-behaved living systems need only an initiator and monomer, as occurs in the anionic polymerization of styrene, dienes, and ethylene oxide. For an increasing number of monomers, more complex processes are needed to retard chain transfer and termination. These systems use initiators, catalysts, and sometimes chain-end stabilizers. The initiator begins chain growth and in all systems is attached (or part of it, at least) to the non-growing chain end. The catalyst is necessary for initiation and propagation but is not consumed. The chain-end stabilizer usually decreases the polymerization rate. When the catalyst is a Lewis acid (electron-pair acceptor), the stabilizer is likely a Lewis base (electron-pair donor), and vice versa. In all systems, the initiation step must be faster than or the same rate as chain propagation to obtain molecular weight control. If the initiation rate is slower than the propagation rate, the first chains formed will be longer than formed the last chains. If an initiator with a structure similar to that of the growing chain is chosen, the initiation rate is assured of being comparable to the propagation rate. A number of living systems operate better if excess

monomer is present. A possible explanation is that the living end is stabilized by complexation with monomer [15]. Large counterions tend to be more effective than small counterions in living polymerization systems even when the ionic center is only indirectly involved.

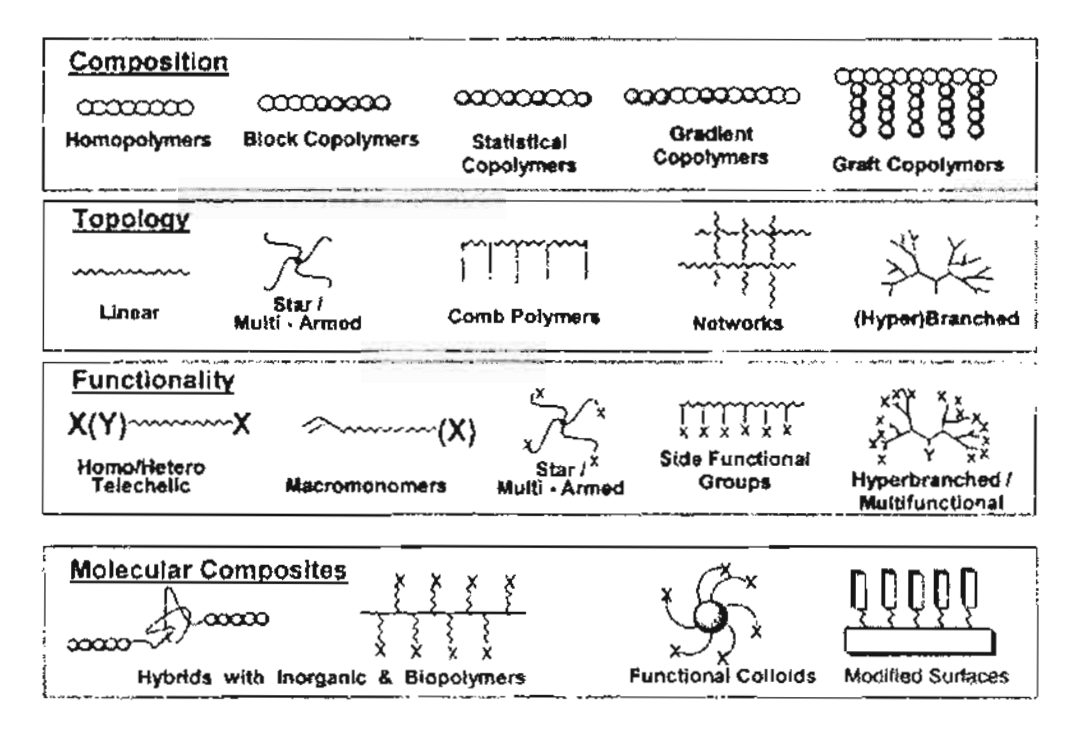


Figure 2.2 Architectural forms of polymers available by living polymerization techniques [15]

In this research, free radical process for living polymerization is selected and described. The concept of using stable free radicals, such as nitroxides, to reversibly react with the growing polymer radical chain end can be traced back to the pioneering work of Mozd and coworkers [16]. After further refinement by Georges [17], the basic blueprint for all subsequent work in the area of "living" free radical polymerization was developed. Subsequently, the groups of Sawamoto [18], Matyjaszewski [19], Percec [20] and others [21-22] have replaced the stable nitroxide free radical with transition metal species to obtain a variety of copper-, nicket-, or ruthenium-mediated "living" free radical systems. These systems are called atom transfer radical polymerization (ATRP). This mechanism is an efficient method for carbon-carbon bond formation in organic synthesis. In some of these reactions, a transition-metal catalyst acts as a carrier of the halogen atom in a reversible redox process (Scheme 2.3). Initially, the transition-metal species, M<sub>t</sub><sup>n</sup>, abstracts halogen atom X from the organic halide, RX, to form the oxidized species, M<sub>t</sub><sup>n+1</sup>X, and the carbon-centered radical R. In the subsequent step, the radical R. participates in inter- or

intramolecular radical addition to alkene, Y, with the formation of the intermediate radical species,  $RY^{\bullet}$ . The reaction between  $M_t^{n+1}X$  and  $RY^{\bullet}$  results in a target product, RYX, and regenerates the reduced transition-metal species,  $M_t^n$ , which further promotes a new redox process. The fast reaction between  $RY^{\bullet}$  and  $M_t^{n+1}X$  apparently suppresses biomolecular termination between alkyl radicals and efficiently introduces a halogen functional group X into the final product in good to excellent yields.

Scheme 2.3 Mechanism of ATRP [19]

The ATRP system relies on one equilibrium reaction in addition to the classical free-radical polymerization scheme (Scheme 2.4). In this equilibrium, a dormant species, RX, reacts with the activator,  $M_t^n$ , to form a radical  $R^{\bullet}$  and deactivating species,  $M_t^{n+1}X$ . The activation and deactivation rate parameters are  $k_{\rm act}$  and  $k_{\rm deact}$ , respectively. Since deactivation of growing radicals is reversible, control over the molecular weight distribution and, in the case of copolymers, over chemical composition can be obtained if the equilibrium meets several requirements [23-24].

- 1. The equilibrium constant,  $k_{\text{act}}/k_{\text{deact}}$ , must be low in order to maintain a low stationary concentration of radicals. A high value would result in a high stationary radical concentration, and as a result, termination would prevail over reversible deactivation.
- The dynamics of the equilibrium must be fast; i.e. deactivation must be fast compared to propagation in order to ensure fast interchange of radicals so as to maintain a narrow molecular weight distribution.

$$R-X + M_t^n - \frac{k_{act}}{k_{deact}} R^{\bullet} + M_t^{n+1}X$$

#### Scheme 2.4 Equilibrium reaction in ATRP [25]

In 1995, Matyjaszewski has described the use of Cu<sup>1</sup>X (X = Br, Cl) with 2,2'-bipyridine (bpy) as a "solubilizing" ligand. The active species has been described as "CuBr·bpy". This system is active toward styrene, acrylates, and methacrylates under the appropriate condition [19]. Percec has also described the role of bpy as partially solubilizing the Cu(I)/Cu(II) catalyst [26]. The role of the bpy is to co-ordinate to Cu(I) to give a pseudo-tetrahedral Cu(I) center in solution (Scheme 2.5).

Scheme 2.5 Rotation of bpy ligand from the tetrahedral to penta-coordinated species when alkyl bromide is incorporated [26]

When uncoordinated, bpy exists predominately in the s-trans conformation in the solid state, in solution there is free rotation with the trans conformation and orthogonal rings are preferred over the cis conformation. Metal complexes contain bpy in a cisoid conformation, forming a planar 5-membered chelating ring. The ligand  $\pi$  orbitals can accept electron density from the metal thus stabilizing low oxidation states, in particular Cu(I). Abstraction by the Cu(bpy)2 cation of halogen atoms from alkyl halides results in oxidation to Cu(II). The penta-coordinated species is shown in Scheme 2.5 which involves rotation of the bpy ligands from the tetrahedral and co-ordination of halide at the Cu center. This has also been proposed by Matyjaszewski [27]. Thus, if this proposed mechanism is correct, the two main roles of the ligand are (i) stabilization of Cu(I) by removal of electron density from the metal and (ii) the ability to interchange between tetrahedral Cu(I) and distorted square based pyramidal Cu(II). Copper (I) halides are very insoluble in organic solvents and monomers, and therefore the concept of solubilizing copper (I) indeed valid. However, the use of either Cu'Br or Cu'Cl wirh bpy under atom transfer radical polymerization conditions results in a very heterogeneous reaction medium with a deep red Cu-(bpy)2 complex in solution and insoluble copper halide visible as a pale green solid. Under these conditions, it is impossible to determine the actual concentration of active catalyst. The system has been modified to give a homogeneous system by the use of

bipyridines with alkyl substituents in the 4<sup>th</sup> position e.g. *tert*-butyl [28-29]. The use of these homogeneous copper (I) complexes results in a marked lowering of the polydispersity index (PDI) to approximately 1.05.

In 2003, Matyjaszewski's group studied the effect of [bpy]/[Cu(I)] ratio, polarity of the medium, and nature of alkyl bromides on the activation rate constants ( $k_{act}$ ) in ATRP. The highest values of  $k_{act}$  for Cu(I)Br were obtained at [bpy]/[Cu(I)Br] ~2/1 and 1/1 in more polar and less polar solvents, respectively. This was ascribed to different structures of the complex, Cu(bpy)<sub>2</sub> Br and Cu(bpy)<sub>2</sub> CuBr<sub>2</sub>, correspondingly (Scheme 2.6) [30].

Scheme 2.6 Complex formation equilibrium in polar and nonpolar solvents [30]

ATRP can be applied to a large variety of monomers [31-34] to produce polymers with well-defined microstructures [22]. The success of ATRP in synthesizing hydrophilic polymers provides an addition advantage over the traditional living ionic polymerization. The first example of aqueous ATRP was reported by Matyjaszewski's group in 1998. They found that ATRP of 2-hydroxyethyl acrylate (HEA) can be carried out directly in water in the presence of CuX/bpy/R-X at 90°C. After polymerization for 12 h, 87% monomer conversion

(Favored in more polar solvents)

was achieved, the molecular weight of the final product was 14,700, and the final polydispersity was 1.34 [35]. Similar results were obtained by Armes's group for the controlled polymerization of sodium methacrylate in water at 90°C. Monomer conversions of 70-80% were achieved after 10 h, with polydispersity of 1,20-1,30 [36]. In 2000, Wang and Armes reported the facile ATRP of methoxy-capped oligo(ethylene glycol) methacrylate (OEGMA) in water at 20°C with various initiators. A remarkably fast rate of polymerization was observed, with unusually high monomer conversions (up to 99%), first-order monomer kinetics, and predetermined molecular weights with narrow molecular weight distributions, indicating good "living" character [37-38]. In 2001, the efficient, controlled polymerization of 2-hydroxyethyl methacrylate (HEMA) is achieved using ATRP in methanol/water mixtures or pure methanol at 20°C by Armes and coworkers [39]. In the same year, Armes's group polymerized to high conversions of the biocompatible polymers based on 2methacryloyloxyethyl phosphorylcholine (MPC) in both aqueous and alcoholic media at ambient temperature via ATRP. Low polydispersities were obtained [40-41]. Furthermore, MPC-based diblock copolymers can also be synthesized via ATRP. For example, an addition of 2-(diethylamino)ethyl methacrylate (DEA) to MPC homopolymer at high conversion in methanol resulted in further chain growth and the formation of an MPC-DEA diblock copolymer. This diblock copolymer dissolved molecularly in acidic solution due to protonation of the DEA residues but formed micelles at pH 8 upon an addition of NaOD [41]. Such micelles are expected to act as "stealthy" nanoparticles, since the MPC block should minimize protein adsorption and hence prevent phagocytosis. The MPC-DEA diblock copolymer coating on PET substrate gave a 76% reduction in fibrinogen binding compared to that with an uncoated substrate. Even greater fibrinogen reduction (up to 85%) was obtained using another MPC-DEA diblock copolymer. Thus, planar surfaces coated with MPC-based copolymers prepared via ATRP are rendered highly biocompatible.

### 2.3 Polymer Brush

Polymer brushes refer to an assembly of polymer chains which are tethered by one end to a surface or an interface [42]. Tethering is sufficiently dense that the polymer chains are crowded and forced to stretch away from the surface or interface to avoid overlapping, sometimes much further than the typical unstretched size of a chain. These stretched configurations are found under equilibrium conditions; neither a confining geometry nor an external field is required. This situation, in which polymer chains stretch along the direction normal to the grafting surface, is guite different from the typical behavior of flexible polymer

chains in solution where chains adopt a random-walk configuration. A series of discoveries show that the deformation of densely tethered chains affects many aspects of their behavior and results in many novel properties of polymer brushes [42].

Polymer brushes are a central model for many practical polymer systems such as polymer micelles, block copolymers at fluid-fluid interfaces (e.g. microemulsions and vesicles), grafted polymers on a solid surface, adsorbed diblock copolymers and graft copolymers at fluid-fluid interfaces. All of these systems, illustrated in Figure 2.3, have a common feature: the polymer chains exhibit deformed configurations. Solvent can be either present or absent in polymer brushes. In the presence of a good solvent, the polymer chains try to avoid contact with each other to maximize contact with solvent molecules. With solvent absence (melt conditions) polymer chains must stretch away from the interface to avoid overfilling incompressible space.

The interface to which polymer chains are tethered in the polymer brushes may be a solid substrate surface or an interface between two liquids, between a liquid and air, or between melts or solutions of homopolymers. Tethering of polymer chains on the surface or interface can be reversible or irreversible. For solid surfaces, the polymer chains can be chemically bonded to the substrate or may be just adsorbed onto the surface. Physisorption on a solid surface is usually achieved by block copolymers with one block interacting strongly with the substrate and another block interacting weakly. For interfaces between fluids, the attachment may be achieved by similar adsorption mechanisms in which one part of the chain prefers one medium and the rest of the chain prefers the other.

Polymer brushes (or tethered polymers) attracted attention in 1950s when it was found that grafting polymer molecules to colloidal particles was a very effective way to prevent flocculation [42]. In other words, one can attach polymer chains which prefer the suspension solvent to the colloidal particle surface; the brushes of two approaching particles resist overlapping and colloidal stabilization is achieved. The repulsive force between brushes arises ultimately from the high osmotic pressure inside the brushes. Subsequently it was found that polymer brushes can be useful in other applications such as new adhesive materials [43-44], protein-resistant biosurfaces [45], chromotographic devices [46], lubricants [47], polymer surfactants [42] and polymer compatibilizers [42]. Tethered polymers which possess low critical solution temperature (LCST) properties exhibit different wetting properties above and below LCST temperature [48]. A very promising field that has been extensively investigated is using polymer brushes as chemical gates. Ito and coworkers [49-51] have reported pH sensitive, photosensitive, oxidoreduction-sensitive

polymer brushes covalently tethered on porous membranes, which are used to regulate the liquid flowing rate through porous membranes. Suter and coworkers [52-53] have prepared polystyrene brushes on high surface area mica for the fabrication of organic-inorganic hybrids. Cation-bearing peroxide free-radical initiators were attached to mica surfaces via ion exchange and used to polymerize styrene. This process is important in the field of nanocomposites. Patterned thin organic films could be useful in microelectronic [54], cell growth control [55-56], biomimetic material fabrication [57], microreaction vessel and drug delivery [58].

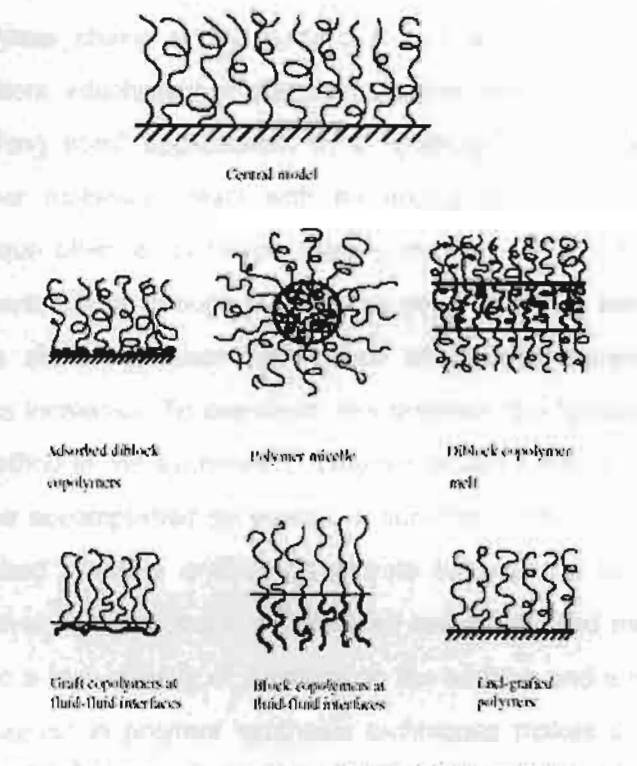


Figure 2.3 Examples of polymer systems comprising polymer brushes

In terms of polymer chemical compositions, polymer brushes tethered on a solid substrate surface can be divided into homopolymer brushes, mixed homopolymer brushes, random copolymer brushes and block copolymer brushes. Homopolymer brushes refer to an assembly of tethered polymer chains consisting of one type of repeat unit. Mixed homopolymer brushes are composed of two or more types of homopolymer chains [59]. Random copolymer brushes refer to an assembly of tethered polymer chains consisting of two different repeat units which are randomly distributed along the polymer chain [60]. Block copolymer brushes refer to an assembly of tethered polymer chains consisting of two or more homopolymer chains covalently connected to each other at one end [61]. Homopolymer brushes can be further divided into neutral polymer brushes and charged

polymer brushes. They may also be classified in terms of rigidity of the polymer chain and would include flexible polymer brushes, semiflexible polymer brushes and liquid crystalline polymer brushes. These different polymer brushes are illustrated in Figure 2.4.

Generally, there are two ways to fabricate polymer brushes: physisorption and covalent attachment (Figure 2.5). For physisorption, block copolymers adsorb onto a suitable substrate with one block interacting strongly with the surface and the other block interacting weakly with the substrate. The disadvantage of physisorption include thermal and solvolytic instabilities due to the non-covalent nature of the grafting, poor control over polymer chain density and complications in synthesis of suitable block copolymers. Tethering of the polymer chains to the surface is one way to surmount some of these disadvantages. Covalent attachment of polymer brushes can be accomplished by either "grafting to" or "grafting from" approaches. In a "grafting to" approach, preformed endfunctionalized polymer molecules react with an appropriate substrate to form polymer brushes. This technique often leads to low grafting density and low film thickness, as the polymer molecules must diffuse through the existing polymer film to reach the reactive sites on the surface. The steric hindrance for surface attachment increase as the tethered polymer film thickness increases. To overcome this problem, the "grafting from" approach is a more promising method in the synthesis of polymer brushes with a high grafting density. "Grafting from" can be accomplished by treating a substrate with plasma or glow-discharge to generate immobilized initiators onto the substrate followed by in situ surface-initiated polymerization. However, "grafting from" well-defined self-assembled monolayers (SAMs) is more attractive due to a high density of initiators on the surface and a well-defined initiation mechanism. Also progress in polymer synthesis techniques makes it possible to produce polymer chains with controllable lengths. Polymerization methods that have been used to synthesize polymer brushes include cationic, anionic, TEMPO-mediated radical, atom transfer radical polymerization (ATRP) and ring opening polymerization.

In order to achieve a better control of molecular weight and molecular weight distribution and to obtain novel polymer brushes like block copolymer brushes, controlled radical polymerizations including ATRP, reverse ATRP, TEMPO-mediated and iniferter radical polymerizations have been used to synthesize tethered polymer brushes on solid substrate surfaces [62-67].

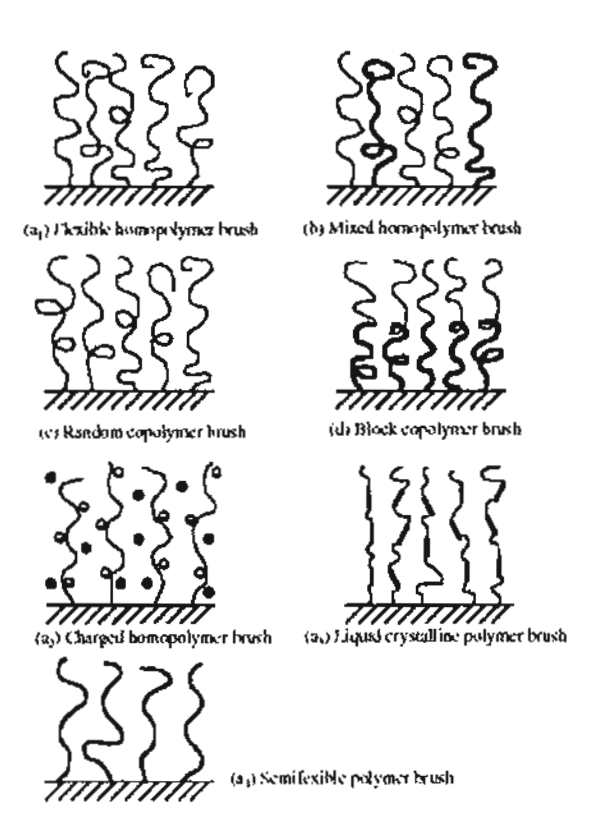


**Figure 2.4** Classification of linear polymer brushes, (a<sub>1</sub>-a<sub>4</sub>) homopolymer brushes; (b) mixed homopolymer brush; (c) random copolymer brush; (d) block copolymer brush

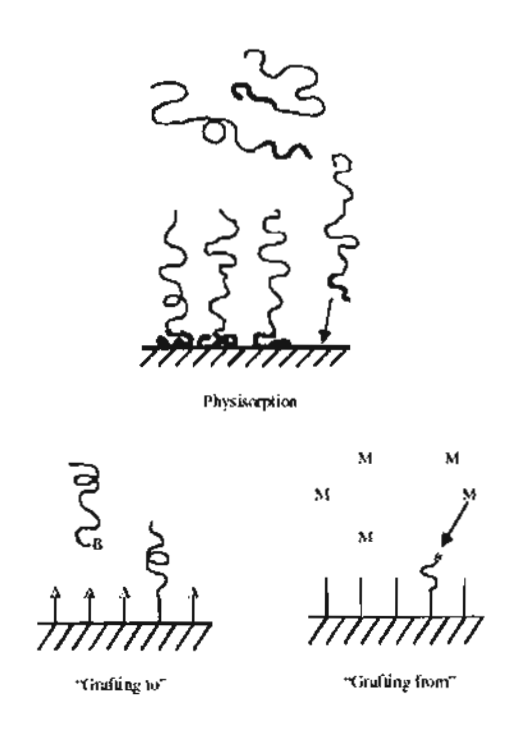


Figure 2.5 Preparation of polymer brushes by "physisorption", "grafting to" and "grafting from"

ATRP is a newly developed controlled radical polymerization [28]. It has attracted considerable attention due to its control of molecular weight, molecular weight distribution and synthesis of block copolymers. Husseman and coworkers [64] applied ATRP in the synthesis of tethered polymer brushes on silicon wafers and achieved great success. They prepared SAMs of 5-trichlorosilylpentyl-2-bromo-2-methylpropionate on silicate substrates. The α-bromoester is a good initiator for ATRP. They have successfully synthesized PMMA brushes by the polymerization of MMA initiated from the SAMs. It has also been reported that tethered polyacrylamide has been obtained from surface initiated ATRP of acrylamide on a porous silica gel surface [65].

Recently, Matyjaszewski and coworkers [68] reported a detailed study of polymer brush synthesis using ATRP. Block copolymers of polystyrene-b-poly(tert-butyl acrylate) on silica wafer have been prepared exclusively by ATRP. Modification of the hydrophilicity of the surface layer was achieved by hydrolysis of the tert-butyl ester to form polystyrene-b-poly(acrylic acid) and confirmed by a decrease in water contact angle from 86° to 18°. On the other hand, high contact angles were obtained when fluoroacrylates were polymerized from the surface (119°).

In 2001, Armes and coworkers synthesized polymer brush by ATRP of 2-hydroxyethyl methacrylate (HEMA) and methoxy-capped oligo(ethylene glycol) methacrylate (OEGMA) from silica modified with an initiator layer composed of 2-bromoisobutylrate. These polymer-grafted silica particles produced in this initial study are fascinating new "model" sterically stabilized colloids which are likely to prove attractive for both theoretical and experimental studies. The aqueous solution properties of the grafted polymer chains determine the colloid stability of the particles, as expected [69].

#### 2.4 Patterned Polymer Film

Artificially designed fine patterning of polymer film has received a great deal of attention in various fields of science and technology such as microelectronics, anti-etching, optical devices, biological and chemical sensors, and tissue engineering. Moreover, their relevance as model heterogeneous systems has led to fundamental understanding of interface phenomena. This growing field has produced a variety of surface patterns at both nanometer and micrometer scales. Thin films of polymers that incorporate reactive functional groups provide a surface that can be further modified by chemical reactions. Methods for attaching polymers to self-assembly monolayer (SAMs) have been continuously developed, for example, electrostatic adsorption of polyelectrolytes to an oppositely charged surface, chemisorption of polymers containing reactive groups to a surface, and covalent

attachment of polymers to reactive SAMs. At present, there are a few methods available for patterning thin films of polymers on SAMs. These include procedures based on photolithography, templating the deposition of polymers using patterned SAMs, and templating phase separation in diblock copolymers.

Recently, polymer brushes have attracted considerable attention for creating patterned surface because of their novel structures and properties. An assembly patterned polymer brushes could be obtained by traditional photolithography or chemical amplification of patterned SAMs.

In 1997, Rühe and coworkers [70] explored preparation of patterned, covalently tethered polymer brushes by photolithography using an appropriate mask and deep or near UV irradiation before, during and after polymer brush formation. Three approaches were attempted. First, surface reactions were carried out to remove tethered polymer chains from selected areas. The second approach used light irradiation to decompose immobilized azo initiators in selected areas followed by polymer brush formation through thermally induced radical polymerization in the unirradiated areas. The third technique was photoactivation of an initiator through a mask leading to photopolymerization in selected areas. All three approaches allowed preparation of patterned, covalently tethered polymer brushes with a high spatial resolution. Using photolithography, Chen and coworkers [71] also obtained micropatterned, immobilized poly(acrylic acid) on a polystyrene film. In 2000, Hawker and coworkers [72] used TEMPO-mediated radical polymerization to prepare a poly(tert-butyl acrylate) brush on a silicate substrate. A polystyrene film containing bis(textbutylphenyl)iodonium triflate was spin-cast onto the polymer brush followed by exposure of the surface to UV radiation through a mask. Photogenerated acid converted poly(tert-butyl acrylate) brushes to poly(acrylic acid) brushes. The end result was a patterned surface containing distinct areas of hydrophobic and hydrophilic brushes.

In 1998, Whitesides and coworkers [73] have introduced the concept of microcontact printing (μCP) to prepare patterned SAMs. This method has been extended into patterning polymer films. Later in 1999 [74], they reported patterned polymer growth on silicon surfaces using μCP and surface-initiated polymerization. μCP was used to prepare a patterned SAM composed of octadecyltrichlorosilane and norbornenyl trichlorosilane. Exposure of the surface to a Ru metathesis catalyst followed by surface-initiated ROMP of norbornene produced patterned polymer brushes. The patterned polymer films were successfully used as reactive ion etching resists. In the same year, Hussemann and coworkers [75] have successfully achieved patterned, covalently tethered polymer brushes

by chemical amplification from patterned SAMs with hydroxyl and methyl terminal groups. Their strategy is illustrated in Figure 2.6. Di(ethylene glycol) and methyl-terminated monolayers were patterned by microcontact printing on gold surface. Surface-initiated ring opening polymerization of ε-carprolactone in the presence of a free initiator such as benzyl alcohol catalyzed by triethylaluminum under suitable conditions produced tethered polymer brushes in the hydroxyl functionalized areas. It was found that the thickness of poly(ε-carprolactone) varied linearly with the Mn of the free polymer formed in solution from the added initiator. In 2000, Shah et al. [76] used ATRP to amplify initiator monolayers prepared by μCP on gold surfaces.

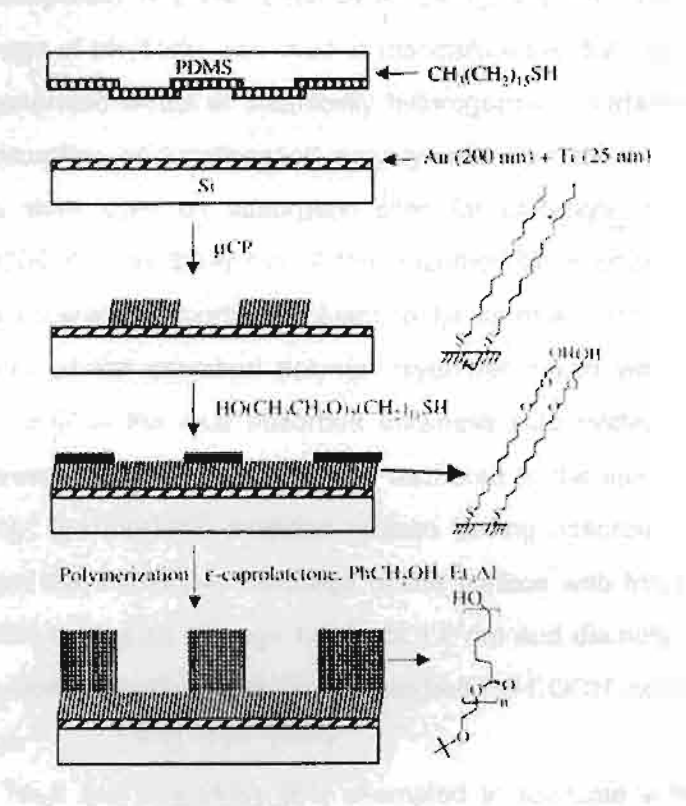


Figure 2.6 Strategy for amplification of a patterned SAM prepared by  $\mu$ CP into a patterned polymer brush

In 1999, Yan et al. [77] described the patterning of poly(ethylene imine) (PEI) on a surface into structures having submicron edge resolution. This patterned thin film of PEI was attached covalently to the SAM by amide bonds. These procedure consists of 3 steps: (1) formation of a reactive SAM terminating in interchain carboxylic anhydride group on gold and silver; (2) patterning of this SAM by  $\mu$ CP using a poly(dimethylsiloxane) stamp linked with PEI; (3) hydrolysis of the unreacted anhydride groups with base and removal of

noncovalently bound PEI. In the same year, Ingall and coworkers [78] reported a method for the production of patterned monolayers that allows the generation of micron sized features by creating a phenylsilane monolayer on the oxide surface and then using 193 nm light to cleave the surface phenyl groups; the remaining groups can then be functionalized to create surface – grafted patterned polymer layers.

Furthermore, McCarthy and Fadeev [79, 80] prepared tris(TMS) monolayers which was used as patterns for the synthesis of uniformly mixed binary monolayers of organosilanes on oxidized silicon wafers. Data from contact angle studies using probe fluids of different sizes suggested that tris(TMS) monolayers have interstitial holes having the size of nanometers (nanopores). Reported Later by McCarthy and coworkers, the controlled over the surface coverage of tris(TMS) was used to manipulate the distribution and size of these nanopores and generated model of chemically heterogeneous surfaces (silanol mixed with tris(TMS)) for adsorption of functionalied polystyrene. Unreacted silanol groups on the substrate surface were used as adsorption sites for carboxylic acid end-functionalized polystyrene (PS-COOH). The thickness of the adsorbed layer could be controlled by the tris(TMS) surface coverage, adsorbing solvent, polymer molecular weight and adsorption time. The thickness of the adsorbed polymer layer decreased with increasing tris(TMS) coverage. An increase in the total adsorbed thickness was evidenced as the molecular weight of the polymer and a number of chains anchored to the surface increased. For the surface topography, the tris(TMS)-modified surface having adsorbed PS-COOH exhibited texture arising from the incomplete coverage of the surface with tris(TMS). Aggregates of adsorbed PS-COOH having an average height of 1.2 nm and diameter of 22 nm were also observed. An average separation distance of adsorbed PS-COOH increased with increasing tris(TMS) coverage.

In 2002, Tsujii and coworkers [81] attempted to fabricate a finely patterned graft layer with a nano-scale resolution by the combined use of surface-initiated living radical polymerization and electron beam lithography; the electron beam was scanned on an initiator-immobilized substrate to selectively bombard and decompose the initiator, followed by the electron beam induced pattern was amplified by the atom transfer radical polymerization (ATRP). This system indicated that increasing electron beam doses was required to cope with the relatively low electron beam sensitivity of the initiators, resulting the graft density of polymer decreased.

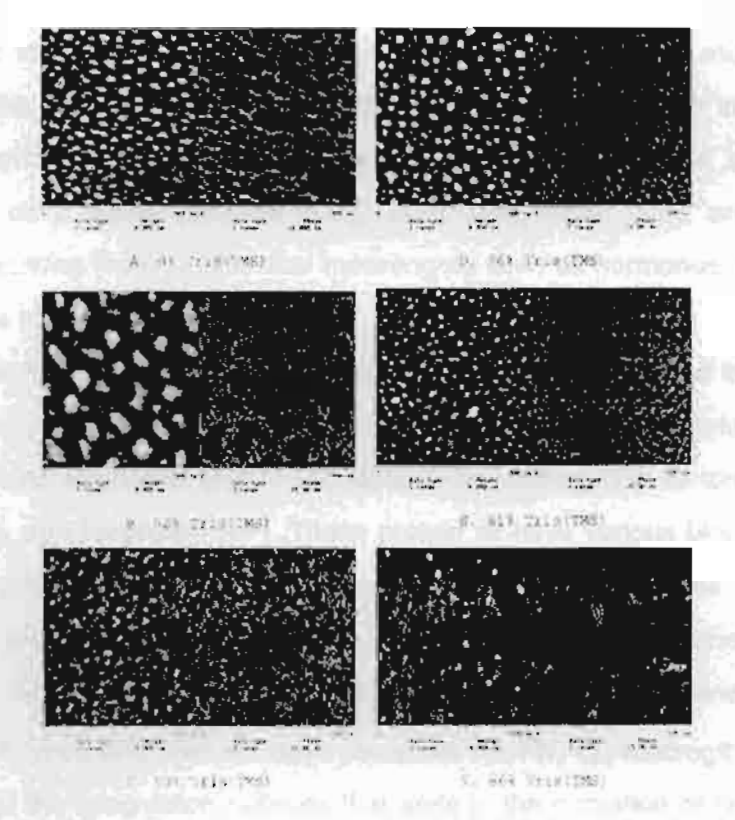


Figure 2.7 AFM images (height/phase) of 11K PS-COOH adsorbed from toluene to tris(TMS) --modified surfaces

#### 2.5 Blood Compatibility [82]

The term "biocompatibility" encompasses many different properties of the materials, however, two important aspects of biomaterial screening refers to their in vitro cytotoxicity and blood compatibility behavior. Artificial surfaces in contact with blood trigger a number of biological systems through the adsorption of protein and cells. It is generally believed that the nature of adsorbed protein layer determines all adverse events that impair the use of artificial materials in medical devices: thrombus formation as a result of platelet adhesion, platelet activation, initiation of coagulation and activation of the complement system that in turn results in leukocyte adhesion and activation.

#### 2.5.1 Human Plasma

Human blood is a highly complex substance. Its major components are red blood cells, which carry oxygen from the lungs to the body; white blood cells, which have major roles in disease prevention and immunity; and platelets, which are key elements in the blood clotting process. These blood elements are suspended in blood plasma, a yellowish liquid that comprises about 55 % of human blood. When the blood was spin in a centrifuge,

the red cells go to the bottom of the container, and the white cells and platelets to the middle, leaving the yellowish plasma at the top. The plasma is the river in which the blood cells travel. It carries not only the blood cells but also nutrients (sugars, amino acids, fats, salts, minerals, etc.), waste products (CO<sub>2</sub>, lactic acid, urea, etc.), antibodies, clotting proteins (called clotting factors), chemical messengers such as hormones, and proteins that help maintain the body's fluid balance.

Many specific functions of blood are carried out by proteins found in plasma. Human plasma contains a number of proteins such as albumin (Alb), immunoglubulins (Ig), complement factors, fibrinogen (Fg), Fibronectin (FN), coagulation factors (activators and down regulators), and lipoprotein (LP). These protein all have various biological role: Alb is considered a biological passivator; immunoglobulin G (IgG) activates the complement system and, for example, binds lymphocytes; the complement factors (including C3) are a part of immune defense ending in the lysis of cells with the membrane attack complex repturing the cell types and bacteria have receptors for FN,  $\Omega_2$ -macroglobulin ( $\Omega_2$ M) is a down regulator of the coagulation cascade that ends in the formation of blood clot in which factors like high molecular weight kininogen (HMWK), factor XII (F XII), factor VII (F VII) and prekallikrein (PK) are component, anti thrombin III (ATh III) is another potent down regulator of coagulation, as it binds thrombin, LP can act as transport protein of such agents as cholesterol.

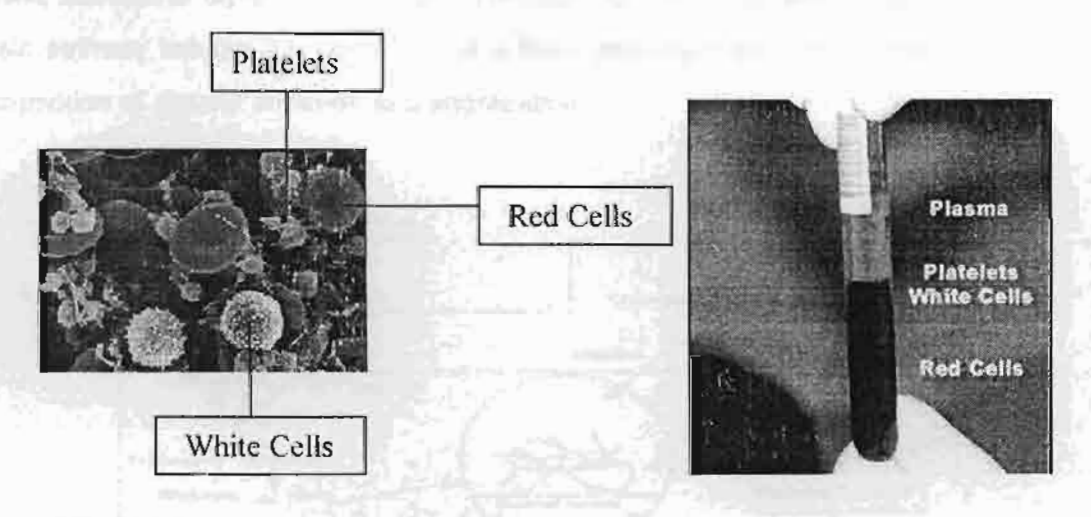


Figure 2.8 Pictorial representation of human blood

### 2.5.2 Mechanism of Thrombus Formation on Polymer Surface

When artificial materials contact a living organism, severe biological responses are induced. Particularly, thrombus is formed when blood encounters a foreign surface as shown in Figure 2.9. The mechanism of coagulation is very complicated, but for simplicity

can be classified into three processes: (1) the coagulation system, (2) the platelet system, and (3) the complemental system. The coagulation system can be further classified into two processes. One is started by Factor VII when the tissue is damaged extrinsically (i.e. outside the body). The other is induced by Factor XII (Hageman Factor) which is activated via an inflammation originating within the body (i.e. intrinsic pathway). It is well known that platelets also contribute to thrombus formation. A foreign substrate induces adhesion and activation of platelets with the adsorbed protein layer serving as a controlling factor of the platelet response. The adhesion of platelets to a biomaterial surface is followed by the platelet release reaction taking place in the adhering platelets and then platelet aggregation on the surface.

The complement system can also be classified into two processes: (1) the classical pathway and (2) the alternative pathway. The classical pathway is started from the interaction between the immunocomplex contained within immunoglobulin G (IgG) or immunoglobulin M (IgM) and C1q in the C1 complex. The alternative pathway is started with C3a work for adhesion of leukocyte and activation of C5.

These three mechanisms of coagulation are not independent. Normally, thrombus formation on a foreign surface results in an interaction between platelets and intrinsic pathway. Initiation of the intrinsic coagulation cascade may be induced by thromboplastins liberated from platelets or by Factor XII activation caused by platelets stimulated by released adenosine diphosphate (ADP). Thrombin formation caused by activation of the intrinsic pathway induces the production of a fibrin monolayer on a biomaterial surface and the promotion of platelet adhesion and aggregation.

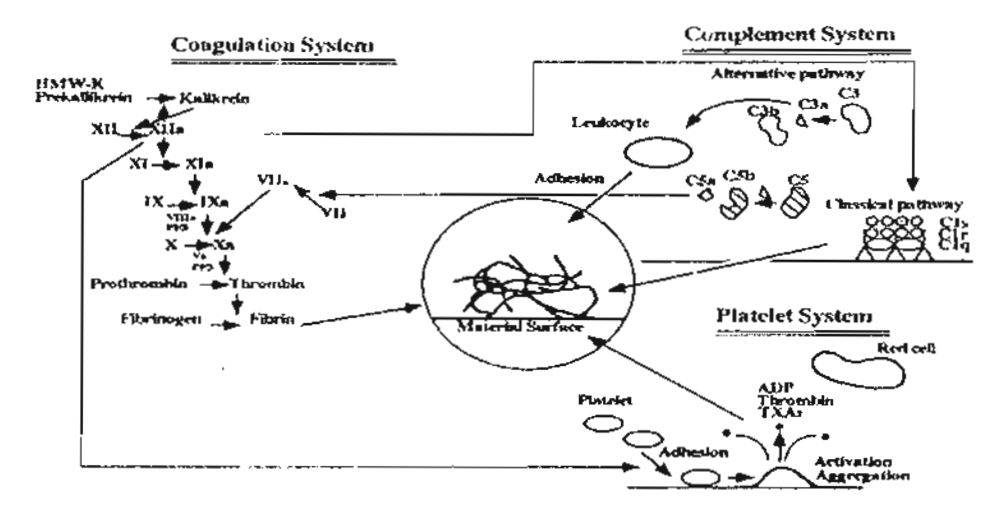


Figure 2.9 Schematic representation of blood coagulation system

### 2.6 Characterization Techniques

### 2.6.1 Ellipsometry [83]

Ellipsometry is a sensitive optical technique for determining properties of surfaces and thin films. If linearly polarized light of a known orientation is reflected at oblique incidence from a surface then the reflected light is elliptically polarized. The shape and orientation of the ellipse depend on the angle of incidence, the direction of the polarization of the incident light, and the reflection properties of the surface. Ellipsometry measures the polarization of the reflected light with a quarter-wave plate followed by an analyzer; the orientations of the quarter-wave plate and the analyzer are varied until no light passes though the analyzer. From these orientations and the direction of polarization of incident light are express as the relative phase change,  $\Delta$ , and the relative amplitude change,  $\Psi$ , introduced by reflection from the surface. These values are related to the ratio of Fresnel reflection coefficients,  $R_{\rm e}$  and  $R_{\rm s}$  for p and s-polarized light, respectively.

$$Tan(\Psi) e^{i\Delta} = \underline{R}_{\varrho}$$

$$R_{s}$$
(2.2)

An ellipsometer measures the changes in the polarization state of light when it is reflected from a sample. If the sample undergoes a change, for example, a thin film on the surface changes its thickness, then its reflection properties is also changed. Measuring these changes in the reflection properties allow us to deduce the actual change in the film's thickness.

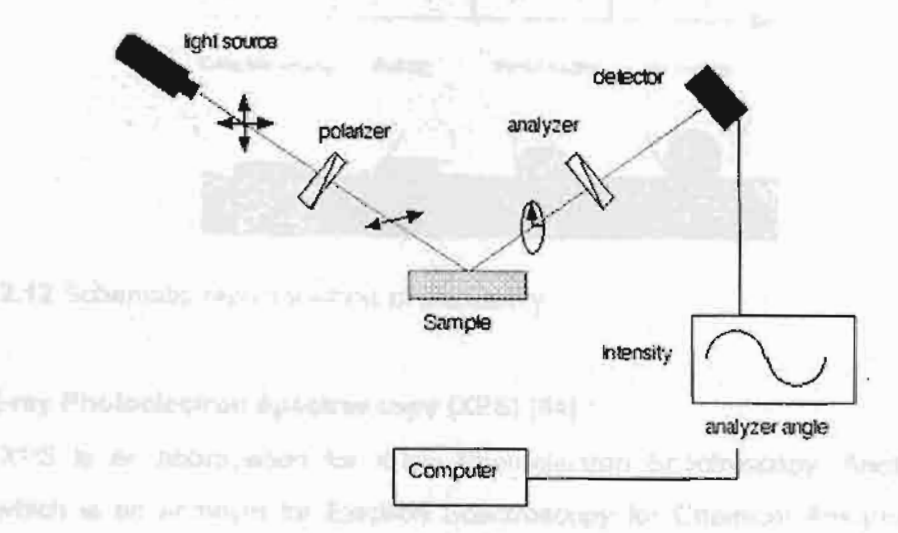


Figure 2.10 Schematic of the geometry of an ellipsometry experiment

buterlai JM, Mr. E. When the Names Restau with

### 2.6.2 Contact Angle Measurement [84]

Contact angle measurements are often used to assess changes in the wetting characteristics of a surface and hence indicate a change in surface energy. The technique is based on the three-phase boundary equilibrium described by Young's equation (Eq. 3).

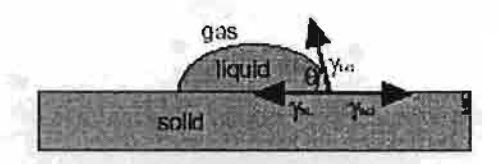


Figure 2.11 Schematic representation of the Young's equation

$$\gamma_{LG}\cos\theta = \gamma_{SG} - \gamma_{SL} \tag{2.3}$$

where  $\gamma_{LG}$ ,  $\gamma_{SG}$  and  $\gamma_{SL}$  are the interfacial tension between the phases with subscripts L, G, S corresponding to liquid, gas, and solid phase, respectively and  $\theta$  refers to the equilibrium contact angle. The Young's equation applies for a perfectly homogeneous atomically flat and rigid surface and therefore supposes many simplifications. In the case of real surfaces, the contact angle value is affected by surface roughness, heterogeneity, vapor spreading pressure, and chemical contamination of the wetting liquid. Although the technique to measure contact angles is easy, data interpretation is not straightforward and the nature of different contributions to the surface is a matter of discussion. Generally, we can define the complete wetting, wetting, partial wetting, and nonwetting according to Figure 2.12.

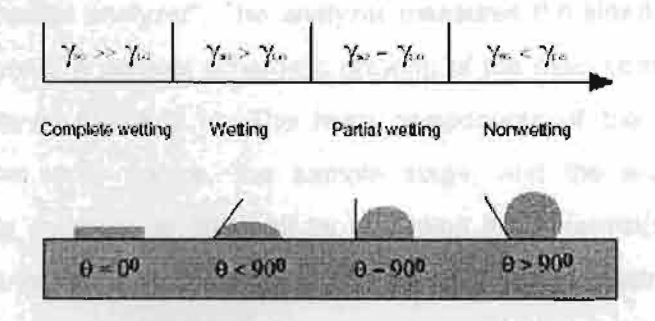


Figure 2.12 Schematic representation of wettability

### 2.6.3 X-ray Photoelectron Spectroscopy (XPS) [84]

XPS is an abbreviation for X-ray Photoelectron Spectroscopy. Another name is ESCA which is an acronym for Electron Spectroscopy for Chemical Analysis. In XPS or ESCA, a beam of (monochromatic) X-rays is first produced by electron bombardment of an anode material (Al, Mg, Si). When the X-rays interact with the sample under investigation,

they can ionize electrons that are in core levels (such as 1s, 2s, etc.). If the binding energy of the electron in the core hole was E<sub>B</sub>, then the kinetic energy of the electron ejected from the surface can be given in the energy diagram (Figure 2.13).

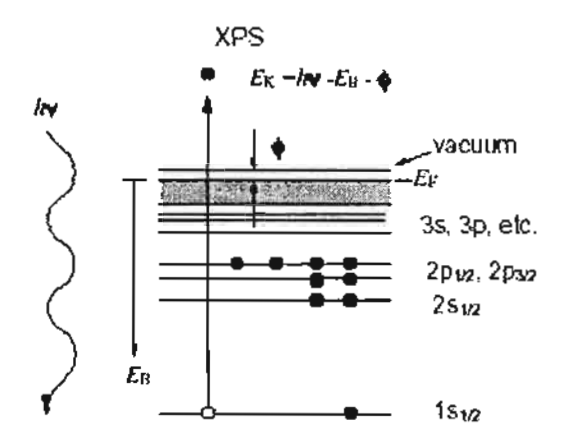


Figure 2.13 Schematic diagram of the X-ray photoelectron emission process

$$E_{K} = h \upsilon - E_{8} - \phi \tag{2.4}$$

where  $E_{\rm K}$  is the measured electron kinetic energy, h v the energy of the exciting radiation,  $E_{\rm B}$  the binding energy of the electron in the solid, and  $\phi$  the spectrometer work function. Since h v is a well-defined quantity, the electron binding energies can be calculated by measuring the kinetic energies of the electrons that are ejected from the sample, using the above equation. The electron energies are measured using an electrostatic energy analyzer such as a "hemispherical analyzer". The analyzer measures the kinetic energy distribution of the emitted electrons. A general schematic drawing of the main components of the XPS instrument is shown in Figure 2.14. The main components of the system include the vacuum system, the x-ray source, the sample stage, and the analyzer. The energy discrimination of the electrons is obtained by sweeping the potential(s) in the lens or by using a grid system in front of the analyzer. The sensitivity of the instrument is dependent on the X-ray source used, the analyzed area, geometrical factors and the efficiencies of the lens, the analyzer and the detector. The energy resolution is due to the inherent width of the X-ray radiation and the resolving power of the spectrometer.

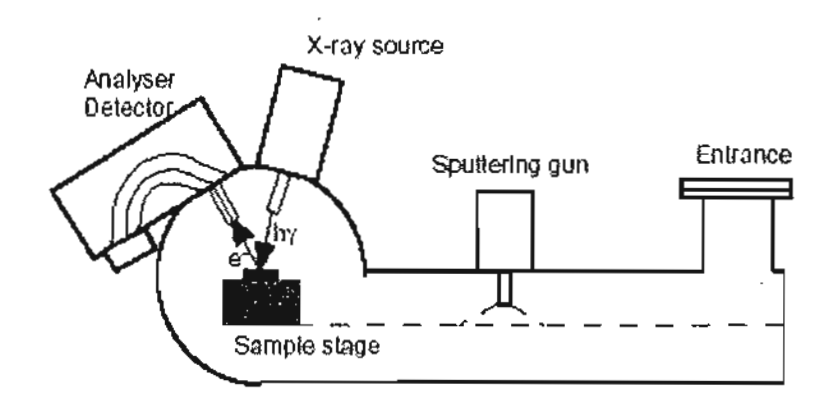


Figure 2.14 General schematic drawing of the XPS instrument

XPS can provide the following information:

- 1. Elemental identification. Because the number of protons increases as we progress through the periodic table, the electron binding energies for a fixed core level (such as the 1s level) will increase monotonically; thus, measuring the electron kinetic energy is equivalent to determining which elements are present on the surface.
- 2. Oxidation states for any given elements. There will be small shifts in the binding energies due to changes in oxidation states; higher oxidation states generally have higher binding energies, and emit electrons with lower kinetic energies.
- Quantitative analyses through curve fitting and calculation of atomic concentrations because the photoelectron intensity is directly related to the atomic concentrations of the photoemitting atoms.
- 4. Depth profiling when combined with ion etching (sputtering) techniques.
- 5. Images or maps showing the distribution of the elements or their chemical states over the surface. Modern instruments can have a spatial resolution down to a few microns.

### 2.6.4 Atomic Force Microscopy (AFM) [85]

Atomic Force Microscope (AFM) is being used to solve processing and materials problems in a wide range of technologies affecting the electronics, telecommunications, biological, chemical, automotive, aerospace, and energy industries. The materials being investigated include thin and thick film coatings, ceramics, composites, glasses, synthetic and biological membranes, metals, polymers, and semiconductors. The AFM is being applied to studies of phenomena such as abrasion, adhesion, cleaning, corrosion, etching, friction, lubrication, plating, and polishing. By using AFM one can not only image the

surface in atomic resolution but also measure the force at nano-newton scale. The publications related to the AFM are growing speedily since its birth.

The first AFM was made by meticulously gluing a tiny shard of diamond onto one end of a tiny strip of gold foil. In 1985, Binnig and Gerber used the cantilever to examine insulating surfaces. A small hook at the end of the cantilever was pressed against the surface while the sample was scanned beneath the tip. The force between tip and sample was measured by tracking the deflection of the cantilever. This was done by monitoring the tunneling current tot a second tip positioned above the cantilever. They could delineate lateral features as small as 300 Å. The force microscope emerged in this way. In fact, without the breakthrough in tip manufacture, the AFM probably would have remained a curiosity in many research groups. It was Albrecht, a fresh graduate student, who fabricated the first silicon microcantilever and measured the atomic structure of boron nitride. Today the tip-cantilever assembly typically is microfabricated from Si or Si<sub>3</sub>N<sub>4</sub>. The era of AFM came finally when the Zurich group released the image of a silicon (111) pattern. The world of surface science knew that a new tool for surface microscope was at hand. After several years the microcantilevers have been perfected, and the instrument has been embraced by scientists and technologists.

The force between the tip and the sample surface is very small, usually less than 10 N. The detection system does not measure force directly. It senses the deflection of the microcantilever. The detecting systems for monitoring the deflection fall into several categories. The first device introduced by Binnig was a tunneling tip placed above the metallized surface of the cantilever. This is a sensitive system where a change in spacing of 1 Å between tip and cantilever changes the tunneling current by an order of magnitude. It is straightforward to measure deflections smaller than 0.01 Å. Subsequent systems were based on the optical techniques. The interferometer is the most sensitive of the optical methods, but it is somewhat more complicated than the beam-bounce method which was introduced by Meyer and Amer. The beam-bounce method is now widely used as a result of the excellent work by Alexander and colleagues. In this system an optical beam is reflected from the mirrored surface on the back side of the cantilever onto a positionsensitive photodetector. In this arrangement a small deflection of the cantilever will tilt the reflected beam and change the position of beam on the photodetector. A third optical system introduced by Sarid uses the cantilever as one of the mirrors in the cavity of a diode laser. Motion of the cantilever has a strong effect on the laser output, and this is exploited as a motion detector

The principles on how the AFM works are very simple. An atomically sharp tip is scanned over a surface with feedback mechanisms that enable the piezo-electric scanners to maintain the tip at a constant force (to obtain height information), or height (to obtain force information) above the sample surface. Tips are typically made from Si<sub>3</sub>N<sub>4</sub> or Si, and extended down from the end of a cantilever. The nanoscope AFM head employs an optical detection system in which the tip is attached to the underside of a reflective cantilever. A diode laser is focused onto the back of a reflective cantilever. As the tip scans the surface of the sample, moving up and down with the contour of the surface, the laser beam is deflected off the attached cantilever into a dual element photodiode. The photodetector measures the difference in light intensities between the upper and lower photodetectors, and then converts to voltage. Feedback from the photodiode difference signal, through software control from the computer, enables the tip to maintain either a constant force or constant height above the sample. In the constant force mode the piezo-electric transducer monitors real time height deviation. In the constant height mode the deflection force on the sample is recorded. The latter mode of operation requires calibration parameters of the scanning tip to be inserted in the sensitivity of the AFM head during force calibration of the microscope.

Some AFM's can accept full 200 mm wafers. The primary purpose of these instruments is to quantitatively measure surface roughness with a nominal 5 nm lateral and 0.01nm vertical resolution on all types of samples. Depending on the AFM design, scanners are used to translate either the sample under the cantilever or the cantilever over the sample. By scanning in either way, the local height of the sample is measured. Three dimensional topographical maps of the surface are then constructed by plotting the local sample height versus horizontal probe tip position.

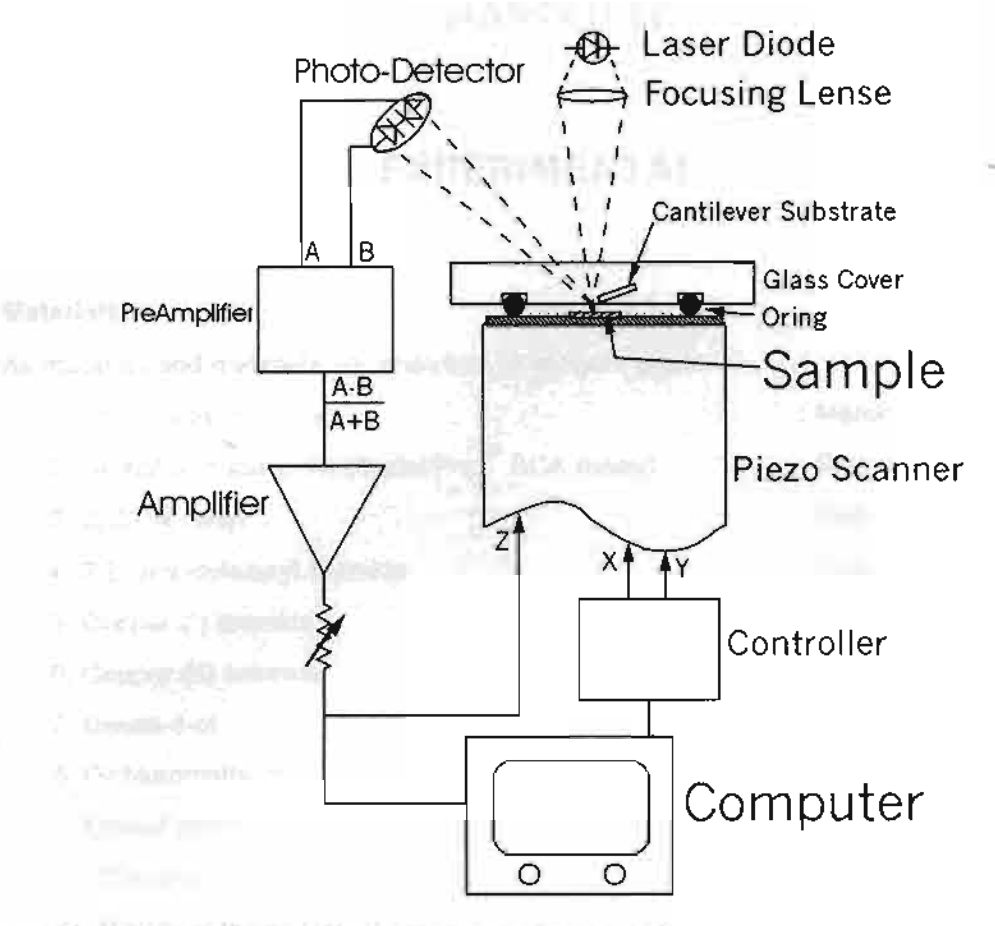


Figure 2.15 Schematic diagram of an atomic force microscope

# **CHAPTER III**

# **EXPERIMENTAL**

### 3.1 Materials

All reagents and materials are analytical or reagent grade.

23. Platelet-poor plasma (PPP)24. Platelet-rich plasma (PRP)

1. Ammonium chloride	: Merck
2. Bicinchonic assay kit (QuantiPro <sup>™</sup> BCA assay)	: Sigma
3. 2, 2'-Bipyridyl	: Fluka
4. 2-Bromoisobutyrył bromide	: Fluka
5. Copper (I) bromide	: Fluka
6. Copper (II) bromide	: Fluka
7. Decen-1-ol	: Aldrich
8. Dichloromethane	: Merck
9. Diethyl ether	: Carlo
10. Dimethoxyethane	; Fluka
11. Dimethylethoxysilane	: Gelest
12. Ethanol	; Merck
13. Ethyl acetate	: Merck
14. Ethyldiisopropylamine	: Fluka
15. Hexane	: Merck
16. Hexen-1-ol	; Aldrich
17. Hydrogen hexachloroplatinate (IV) hexahydrate	: Aldrich
18. Hydrogen peroxide	: Univar
19. Magnesium sulfate anhydrous	: Unilab
20. 2-Methacryloyloxyethyl phosphorylcholine	: NOE corporation, Japan
21. Methanol	: Merck
22. Phosphate buffer saline (PBS)	: Aldrich

: Thai Red Cross Society

: Thai Red Cross Society

25. 1-Propanol : Univar

26. Propen-1-ol : Merck

27. Protein standard (Bovine Serum Albumin: BSA) : Sigma

28. Silica gel 60 (0.063-0.200 mm) : Merck

29. Silicon wafer (Single-sided, polished) : Siltron Inc. Korea

30. Silicon wafer (Double-sided, polished) : Siltron Inc. Korea

31. Sodium dodecyl sulfate : Fluka

32. Sodium sulfate anhydrous : Fluka

33. Sulfuric acid : Merck

34. Tetrahydrofuran : Carlo

35. Tris(trimethylsiloxy)chlorosilane : Gelest

36. Toluene : Carlo

37. Toluene anhydrous 99 % : Aldrich

38. Triethylamine : Carlo

39. Ultrapure distilled water : Mill-Q Lab system

### 3.2 Equipments

### 3.2.1 Ellipsometry

The ellipsometry was studied by using L115C WAFER<sup>TM</sup> ELLIPSOMETER. The thicknesses were determined in air with a  $70^{\circ}$  of incidence angle at 632.8 nm. The thickness of the adsorbed film was calculated using the software "Dafibm" Rudolph Research, Double Absorbing Films Calculations. The calculation was based on a refractive index  $N_{initiator} = 1.443$ ,  $N_{MPC} = 1.488$ ,  $N_{MMA} = 1.460$ ,  $N_{hydroxyl} = 1.462$ ,  $N_{tris(TMS)} = 1.386$  and a silicon substrate refractive index  $N_{substrate} = 3.858$ . At least five different locations on each sample were measured and the average thickness was calculated.

### 3.2.2 X-ray Photoelectron Spectroscopy (XPS)

X-ray photoelectron spectra were collected using ESCA-200, SCIENTA, Uppsala, Sweden. In this study, the take off angle at 15° and 75° were chosen and the approximation of depth profile is ~10 and ~40 Å, respectively.

### 3.2.3 Nuclear Magnetic Spectroscopy (NMR)

The  $^1$ H NMR spectra and  $^{13}$ C NMR spectra were recorded in either CDCl<sub>3</sub>, D<sub>2</sub>O or CD<sub>3</sub>OD using a Varian, model Mercury-400 nuclear magnetic resonance spectrometer operating at 400 MHz. Chemical shifts ( $\delta$ ) are reported in part per million (ppm) relative to tetramethylsilane (TMS) or using the residual protonated solvent signal as a reference.

### 3.2.4 Gel Permeation Chromatography (GPC)

The molecular weight and molecular weight distributions of the MPC homopolymers were determined by aqueous get permeation chromatography (GPC), using Shodex Ohpak SB-803 HQ column connected to the RI detector. The flow rate was 0.5 mL/min. The eluent was water including 10 mM LiBr. Calibration was based on poly(ethylene glycol)(PEG) standards ranging from 6,000 to 50,000 g mol<sup>-1</sup>.

### 3.2.5 Freeze Dryer

Freeze dryer model Freezone 77520, Benchtop, Labconco was used for drying the MPC homopolymers.

#### 3.2.6 Contact Angle Measurements

Contact angle meter (model FACE, Japan) was used for the determination of water contact angles. A droplet of testing Milli-Q water is placed on the tested surface by bringing the surface into contact with a droplet suspended from a needle of the syringe. The measurements were carried out in air at room temperature. Dynamic advancing and receding angles were recorded while water was added to and withdrawn from the drop, respectively. The reported angle is an average of 5 measurements on different areas of each sample.

### 3.2.7 UV-Spectroscopy

UV on Microtiter plate reader, model Sunrise, Tecan Austria GmbH, was used for determining the amounts of the absorbed protein using bicinconic assay by reading UV absorbance at  $\lambda$  = 562 nm.

### 3.2.8 Scanning Electron Microscopy (SEM)

Scanning electron microscopy (SEM) model JSM-5800L, was used to observe the morphology of surface-adherent platelets.

### 3.2.9 Atomic Force Microscopy (AFM)

AFM images were recorded with Atomic Force Microscope model SPI-3800, Seiko I, Tokyo, Japan. Measurements were performed in air using tapping mode. Silicon nitride tip with a resonance frequency of 13 kHz and a spring constant 0.02-0.1 N/m were used.

#### 3.3 Procedures

### 3.3.1 Synthesis of Vinyl-terminated $\alpha$ -Bromoisobutyrate Compounds

To a solution of 25 mmol of propen-1-ol (1.70 mL), hexen-1-ol (4.44 mL) or decen-1-ol (4.46 mL) in 25 mL of tetrahydrofuran, pyridine (2.1 mL, 26.5 mmol) was added followed by a dropwise addition of 2-bromoisobutyryl bromide (3.10 mL, 25 mmol). The mixture was stirred at room temperature overnight, diluted with hexane and then washed with 2N HCl and twice with deionized water. The organic phase was dried over sodium sulfate and filtered. After the solvent was removed from the filtrate under reduced pressure, the colorless oily residue was purified by filtering through a silica gel column chromatography to give the product 1, 2, and 3 in 90, 85, and 85 % yield, respectively.

<sup>1</sup>H NMR (CDCl<sub>3</sub>) of 1 (n = 3):  $\delta$  1.98 (6H, C(CH<sub>3</sub>)<sub>2</sub>, s), 4.71 (2H, OCH<sub>2</sub>, d, J = 5.46 Hz), 5.30-5.44 (2H, =CH<sub>2</sub>, complex m), 5.93-6.0 (1H, =CH, complex m).

<sup>1</sup>H NMR (CDCl<sub>3</sub>) of 2 (n = 6):  $\delta$  1.90 (6H, C(C<u>H</u><sub>3</sub>)<sub>2</sub>, s), 4.14 (2H, C<u>H</u><sub>2</sub>COO, d, J = 6.45 Hz), 2.09 (2H, C=C<u>H</u><sub>2</sub>CH<sub>2</sub>, d, J = 7.04 Hz), 1.47 – 1.66 (4H, C<u>H</u><sub>2</sub>C<u>H</u><sub>2</sub>, d, J = 6.45 Hz),4.96-5.04 (2H, =C<u>H</u><sub>2</sub>, complex m), 5.69-5.86 (1H, =C<u>H</u>, complex m).

<sup>1</sup>H NMR (CDCI<sub>3</sub>) of 3 (n = 10):  $\delta$  1.88 (6H, C(CH<sub>3</sub>)<sub>2</sub>, s), 4.14 (2H, CH<sub>2</sub>COO, d, J = 6.44 Hz), 1.20-1.41 (12H, (CH<sub>2</sub>)<sub>6</sub>, d, J = 5.86 Hz), 4.87-4.99 (2H, =CH<sub>2</sub>, complex m), 2.00 (2H, C=CH<sub>2</sub>CH<sub>2</sub>, complex m), 5.71-5.81 (1H, =CH, complex m).

# 3.3.2 Synthesis of Silane Compounds by Hydrosilylation of Vinyl-terminated $\alpha$ -Bromoisobutyrate Compounds

dimethylethoxysilane bromoisobutyrate derivatives
1.2.3

derivatives of initiator

4.5.6

1 (87.52 mg, 4.23 mmol), 2 (105.28 mg, 4.23 mmol) or 3 (128.97 mg, 4.23 mmol) and dimethylethoxysilane (0.17 mL, 42.6 mmol) were mixed in a dry flask followed by an addition of 0.2 mL of 1:1 ethanol/dimethoxyethane solution of chloroplatinic acid, H<sub>2</sub>PtCl<sub>6</sub> (1.1 mg, 0.002 mmol). The reaction mixture was stirred at room temperature under nitrogen atmosphere in the dark for 14 h. Dry toluene (3 mL) was then added and the excess dimethylethoxysilane was removed under reduced pressure. Dry dichloromethane was added and then removed under reduced pressure. The crude product was passed through a short column of dry sodium sulfate, the column was washed with dry dichloromethane and the dichloromethane was removed under reduced pressure to give the desired product as yellow viscous liquid 4, 5, and 6 in 93, 90, and 90 % yield, respectively.

<sup>1</sup>H NMR (CDCl<sub>3</sub>) of 4 (n = 3):  $\delta$  0.04 (6H, Si(CH<sub>3</sub>)<sub>2</sub>, s), 0.93 (2H, OCH<sub>2</sub> CH<sub>2</sub>CH<sub>2</sub>, t, J = 7.04 Hz ), 1.24 (3H, SiOCH<sub>2</sub>CH<sub>3</sub>, t, J = 7.04 Hz), 1.66 (2H, OCH<sub>2</sub>CH<sub>2</sub>CH<sub>2</sub>, complex m), 1.88 (6H, C(CH<sub>3</sub>)<sub>2</sub>, s), 3.60 (2H, SiOCH<sub>2</sub>CH<sub>3</sub>, q, J = 6.45 Hz), 4.06 (2H, OCH<sub>2</sub>CH<sub>2</sub>CH<sub>2</sub>, t, J = 6.45 Hz).

<sup>1</sup>H NMR (CDCl<sub>3</sub>) of 6 (n = 10):  $\delta$  0.05 (6H, Si(C<u>H</u><sub>3</sub>)<sub>2</sub>, s), 1.22 (3H, SiOCH<sub>2</sub>C<u>H</u><sub>3</sub>, s), 1.3 (16H, OCH<sub>2</sub>CH<sub>2</sub>(C<u>H</u><sub>2</sub>)<sub>8</sub>, s), 1.64 (2H, OCH<sub>2</sub>C<u>H</u><sub>2</sub>(CH<sub>2</sub>)<sub>8</sub>, q, J = 7.03 Hz), 1.89 (6H, C(C<u>H</u><sub>3</sub>)<sub>2</sub>, s), 3.69 (2H, SiOC<u>H</u><sub>2</sub>CH<sub>3</sub>, q, J = 7.03 Hz), 4.13 (2H, OC<u>H</u><sub>2</sub>CH<sub>2</sub>(CH<sub>2</sub>)<sub>8</sub>, t, J = 7.03 Hz).

### 3.3.3 Synthesis of Prop-2-bromo-2-methylpropionate as a "Sacrificial" Initiator

$$OH + Br C Br OCH_3 pyridine CH_3$$

$$CH_3 THF$$

$$CH_3$$

To a solution of 25 mmol of propanol in 25 mL of tetrahydrofuran, pyridine (3.1mL, 26.5 mmol) was added, followed by a dropwise addition of 2-bromoisobutyryl bromide (3.10 mL, 25 mmol). The mixture was stirred at room temperature overnight and then diluted with hexane and washed with 2N HCl and twice with deionized water. The organic phase was dried over sodium sulfate and filtered. The solvent was removed from the filtrate under reduced pressure, and the colorless oily residue was purified by filtering through a silica gel column chromatography to give product in 90% yield.

<sup>1</sup>H NMR (CDCI<sub>3</sub>) of 7 :  $\delta$  1.0 (3H, OCH<sub>2</sub>CH<sub>2</sub>CH<sub>3</sub>, t, J = 7.02 Hz), 1.72 (2H, OCH<sub>2</sub>CH<sub>2</sub>CH<sub>3</sub>, complex m), 1.95 (6H, C(CH<sub>3</sub>)<sub>2</sub>, s), 4.15 (2H, OCH<sub>2</sub>CH<sub>2</sub>CH<sub>3</sub>, t, J = 6.24 Hz).

### 3.3.4 Pretreatment of Silicon Substrates

Silicon wafers were cut into 1.5 x 1.5 cm<sup>2</sup> substrates. The substrates held in a slotted hollow glass cylinder (custom designed holder) were put in a freshly prepared mixture of 7 parts of concentrated sulfuric acid and 3 parts of 30% hydrogen peroxide. Substrates were submerged in the solution at room temperature for 2 h, rinsed with five to seven aliquots of deionized water and placed in a clean oven at 120 °C for 2 h. Silanization reaction was carried out immediately after treating the substrates in this fashion.

### 3.3.5 Preparation of Silicon -supported Mixed Tris(TMS)/silanol Monolayer

Cleaned and dried silicon substrates held in a slotted hollow glass cylinder were covered with 10 mL of anhydrous toluene containing ethyldiisopropylamine (0.17 mL, 1mmol) in a Schlenk flask. Tris(trimethylsiloxy) chlorosilane (tris(TMSCI)) (0.35 mL, 1mmol), was added by syringe. Reactions were carried out at 60 - 70 °C for a predetermined period of time (1, 2, 3 and 4 days) under nitrogen atmosphere. The substrates were rinsed with 1 x 10 mL of toluene, 2 x 10 mL of 2-propanol, 2 x 10 mL of ethanol, 1 x 10 mL of ethanol-water (1:1), 1 x 10 mL of water and 1 x 10 mL of ethanol and then were dried in an oven at 120 °C for 10 min.

# 3.3.6 Preparation of Silicon-supported ∞-Bromoisobutyrate Monolayer and Silicon-supported Mixed Tris(TMS)/∞-Bromoisobutyrate Monolayer

tris(TMS) / 2-bromoisobutyrate mixed surface

9

Cleaned and dried silicon substrates or silicon-supported mixed tris(TMS)/silanol monolayer held in a slotted hollow glass cylinder were covered with 10 mL of anhydrous toluene containing ethydiisopropylamine (0.17 mL, 1 mmol) in a Schlenk flask. 3-(Dimethylethoxysilyl)alkyl-2-bromoisobutyrate (4, 5, or 6, 0.15 mmol) was added by syringe. Reactions were carried out under nitrogen atmosphere at ambient temperature for varying reaction time (1 – 4 days). The substrates were rinsed with 1 x 10 mL of toluene, 2 x 10 mL of 2-propanol, 2 x 10 mL of ethanol, 1 x 10 mL of ethanol-water (1:1), 1 x 10 mL of water and 1 x 10 mL of ethanol and dried under vacuum.

## 3.3.7 Surface-initiated Polymerization of 2-methacryloyloxyethyl phosphoryicholine) (MPC)

PMPC brush on silicon-supported α-bromoisobutyrate monolayer

PMPC brush on silicon-suppoted mixed tris(TMS) / 2-bromoisobutylate

Mixed solvents (methanol / water in 4: 1 ratio) or pure methanol was used as a solvent for polymerization. All solvents were distilled, degassed by two freeze-pump-thaw cycles and purged with nitrogen gas to eliminate oxygen before used. Copper (I) bromide (29 mg, 0.20 mmol) and 2,2′-bipyridyl (63 mg, 0.40 mmol) were dissolved in a Schlenk flask containing 12 mL of methanol. The solution was stirred under nitrogen at 0°C before 6 mL of water was added. In the case of pure methanol, a total of 15 mL methanol was used for solubilizing reagents. Then, propyl-2-bromoisobutylrate (7) (10 μL, 0.060 mmol) was added as a sacrificial initiator. After stirring for 30 min under nitrogen atmosphere, silicon-supported ∞-bromoisobutyrate monolayer or silicon-supported mixed tris(TMS)/∞-bromoisobutyrate

monolayer held in a slotted hollow glass cylinder was then submerged into the flask. MPC (3.6 g, 0.012 mol) was dissolved separately in 12 mL of methanol and purged with nitrogen for 1 h. In the case of pure methanol, 15 mL of methanol was used for solubilizing MPC. The MPC solution was added into the flask and polymerization was carried out at room temperature while stirring under nitrogen atmosphere. The silicon substrates were then removed from the polymerization mixture after the desired reaction time, rinsed with copious amount of methanol and water, respectively before soxhlet-extracted by methanol for 24h and dried under vacuum. PMPC formed in the solution from the "added" initiator was precipitated in cold THF. The viscous PMPC was re-dissolved in deionized water. The PMPC solution was past through a silica column to remove copper catalyst before subjected to dialysis and freeze-dried.

### 3.4 Protocol for Blood Compatibility Test

### 3.4.1 Determination of Total Amount of Adsorbed Human Plasma Protein

The substrates bearing polymer brushes having the dimension of 1.5 x 1.5 cm2 were placed into a 24-well tissue culture plate containing deionized water in each well. The samples were allowed to stand in the wells overnight to reach an equilibrium hydration. Each sample was removed from deionized water and suspended in the wells containing 3.0 mL platelet-poor plasma (PPP) before being incubated at 37°C for 3 h. Three pieces of samples were analyzed for each condition. The samples were removed from PPP and rinsed thoroughly with phosphate buffer saline solution (PBS) (2x) to remove any loosely attached protein. The adsorbed protein on the sample surface was detached by soaking each sample in 3.0 mL of 1 % aqueous solution of sodium dodecyl sulfate (SDS) for 30 min. A protein analysis kit based on the bicinchonic acid (BCA) method was used to determine the concentration of the protein dissolved in the SDS solution. 100 µL (0.1 mL) of SDS solution that soak each sample was added into 96-designated wells. 100 µL of BCA working solution was then added in each well, before the well-plate was incubated at 37°C for 2 h. The absorbance of the solution was measured at 562 nm by UV plate reader. The amount of protein adsorbed on the samples was calculated from the protein concentration in the SDS solution. The data are expressed as mean ± standard deviation (S.D).

#### 3.4.2 Evaluation of Platelet Adhesion

The substrates bearing polymer brushes having the dimension of 1.5 x 1.5 cm<sup>2</sup> were placed in 24-well tissue culture plate containing PBS in each well. The samples were allowed to stand in the wells overnight to reach an equilibrium hydration. The platelet-rich plasma (PRP) (3.0 mL) was added into each well by a micropipet. The well plate was incubated for 1 h at 37 °C. After the PRP was removed using a micropipet, the substrates were rinsed with PBS (3x). The saline solution containing 2.5 % (v/v) glutaraldehyde was added to each well in order to fix the platelets adhered on the sample surfaces. The samples were rinsed with PBS (3x) followed by delonized water (3x) prior to dehydration by sequentially soaking in 30, 50, 70, 90, 99 and 100 % (v/v) ethanol in water for an interval of 10 min. The samples were dried under vacuum for 24 h then sputtered with gold before analyzed by scanning electron microscopy (SEM).

### CHAPTER IV

### RESULTS AND DISCUSSION

In this chapter, the results are divided into five sections. The first section mainly focuses on the synthesis of ∝-bromoisobutyrate-containing silane compounds having different alkyl spacer to be used as surface-tethered initiators. The second section is devoted to the preparation and characterization silicon-supported tris(trimethylsiloxy)silyl of mixed (tris(TMS))/silanol monolayer and subsequent silicon-supported mixed tris(TMS)/∞bromoisobutyrate monolayer which is later used as patterns for the synthesis of surfacetethered polymer brushes. The third section involves surface-initiated polymerization of 2methacryloyloxyethyl phosphorylcholine (MPC) by atom transfer radical polymerization (ATRP) from both silicon-supported ∝-bromoisobutyrate monolayer and silicon-supported mixed tris(TMS)/∞-bromoisobutyrate monolayer. The fourth section explains how the graft density of monolayer influences the morphology of surface-tethered polymer brushes. And the final section addresses biocompatibility of surface-tethered polymer brushes as a function of the thickness and graft density of polymer brushes in terms of plasma protein adsorption and platelet adhesion.

### 4.1 Synthesis of Ct-Bromoester Derivatives to be used as Initiators

Esterification of vinyl-terminated alcohols with 2-bromoisobutyryl bromide was followed by hydrosilylation with dimethylethoxysilane to yield silane compounds having one end capable of bonding to silanol groups on silicon surface and the other end carrying latent  $\alpha$ -bromoester which can later be used to initiate the ATRP of MPC.

### 4.1.1 Synthesis of Vinyl-terminated α-Bromoisobutyrate Compounds

Three analogous vinyl-terminated alcohols (n = 3, 6, and 10) were used as substrates for this reaction. The nucleophilic substitution of vinyl-terminated alcohols with 2-bromoisobutyryl bromide in tetrahydrofuran gave vinyl-terminated  $\alpha$ -bromoisobutyrate compounds as colorless liquid products, which were sufficiently pure for the next synthesis without further purification after the work-up process. The characteristic <sup>1</sup>H NMR peaks and %yield of products are listed in Table 4.1. Singlet signals of the methyl proton of  $C(C\underline{H}_3)_2$  at 1.98, 1.90, 1.88 ppm for products 1, 2, and 3 represented the success of the reactions between vinyl-terminated alcohols and 2-bromoisobutyryl bromide. <sup>1</sup>H NMR spectra of product 1, 2, and 3 are displayed in Figure 4.1, 4.2, and 4.3, respectively.

Table 4.1 Characteristic <sup>1</sup>H NMR peaks and %yield of vinyl-terminated α-bromoisobutyrate compounds

Product No.	Name	Characteristic	% Yield			
	<sup>1</sup> H NMR peaks					
1 (n = 3)	Prop-2'-enyl-2- bromoisobutyrate	singlet of C(CH <sub>3</sub> ) <sub>2</sub> at 1.98 ppm	90			
2 (n = 6)	Hex-5-enyl-2- bromoisobutyrate	singlet of C(CH <sub>3</sub> ) <sub>2</sub> at 1.90 ppm	85			
3 (n = 10)	Dec-9-enyl-2- bromoisobutyrate	singlet of C(CH <sub>3</sub> ) <sub>2</sub> at 1.88 ppm	85			

# 4.1.2 Synthesis of Silane Compounds by Hydrosilylation of Vinyl-terminated $\alpha$ -Bromoisobutyrate Compounds

1,2,3 4,5,6

Hydrosilylation of dimethylethoxysilane with vinyl-terminated  $\alpha$ -bromoisobutyrate compound (1, 2, or 3) was carried out in the dark in the presence of chloroplatinic acid, H<sub>2</sub>PtCl<sub>6</sub> at room temperature for 24 h. Scheme 4.1 illustrates hydrosilylation mechanism using chloroplatinic acid as a catalyst. The reactions yielded yellow viscous liquid as crude products which were sufficiently pure for the next synthesis without further purification after the work-up process. <sup>1</sup>H NMR spectra of the resulting silane compounds (Figures 4.1-4.3) show methyl protons of C(CH<sub>3</sub>)<sub>2</sub> adjacent to bromine at 1.89, 1.93, 1.96 ppm for product 4, 5, and 6, respectively together with the absence of signals from alkene proton (CH<sub>2</sub>=CH) and (CH<sub>2</sub>=CH) previously appeared in vinyl-terminated  $\alpha$ -bromoisobutyrate reactants in the range of 4-6 ppm, indicating that the reactions were complete and gave desirable silane compounds.

$$[Pt] \qquad \qquad H \longrightarrow SiR_2R'$$

$$R = CH_3$$

$$R' = OCH_2CH_3$$

$$R' = CH_2OCC(CH_3)_2Br$$

$$SiR_2R'$$

$$R_2R'Si$$

$$R_2R'Si$$

$$R_3C_2O-Si$$

$$CH_3$$

$$CH_3$$

$$CH_3$$

Scheme 4.1 Mechanism of hydrositylation using chloroplatinic acid as a catalyst

Table 4.2 Characteristic <sup>1</sup>H NMR peaks and %yield of silane compounds

Product	Name	Characteristic	% Yield	
No.		<sup>1</sup> H NMR peaks		
4 (n = 3)	3-(Dimethylethoxysilyl)propyl- 2-bromoisobutyrate	singlet of $C(C\underline{H}_3)_2$ at 1.89 ppm and singlet of $Si(C\underline{H}_3)_2$ at 0.04 ppm	93	
5 (n = 6)	6-(Dimethylethoxysilyl)hexyl-2- bromoisobutyrate	singlet of $C(C\underline{H}_3)_2$ at 1.93 ppm and singlet of $Si(C\underline{H}_3)_2$ at 0.06 ppm	90	
6 (n = 10)	10-(Dimethylethoxysilyi)decyl- 2-bromoisobutyrate	singlet of $C(C\underline{H}_3)_2$ at 1.96 ppm and singlet of $Si(C\underline{H}_3)_2$ at 0.05 ppm	90	

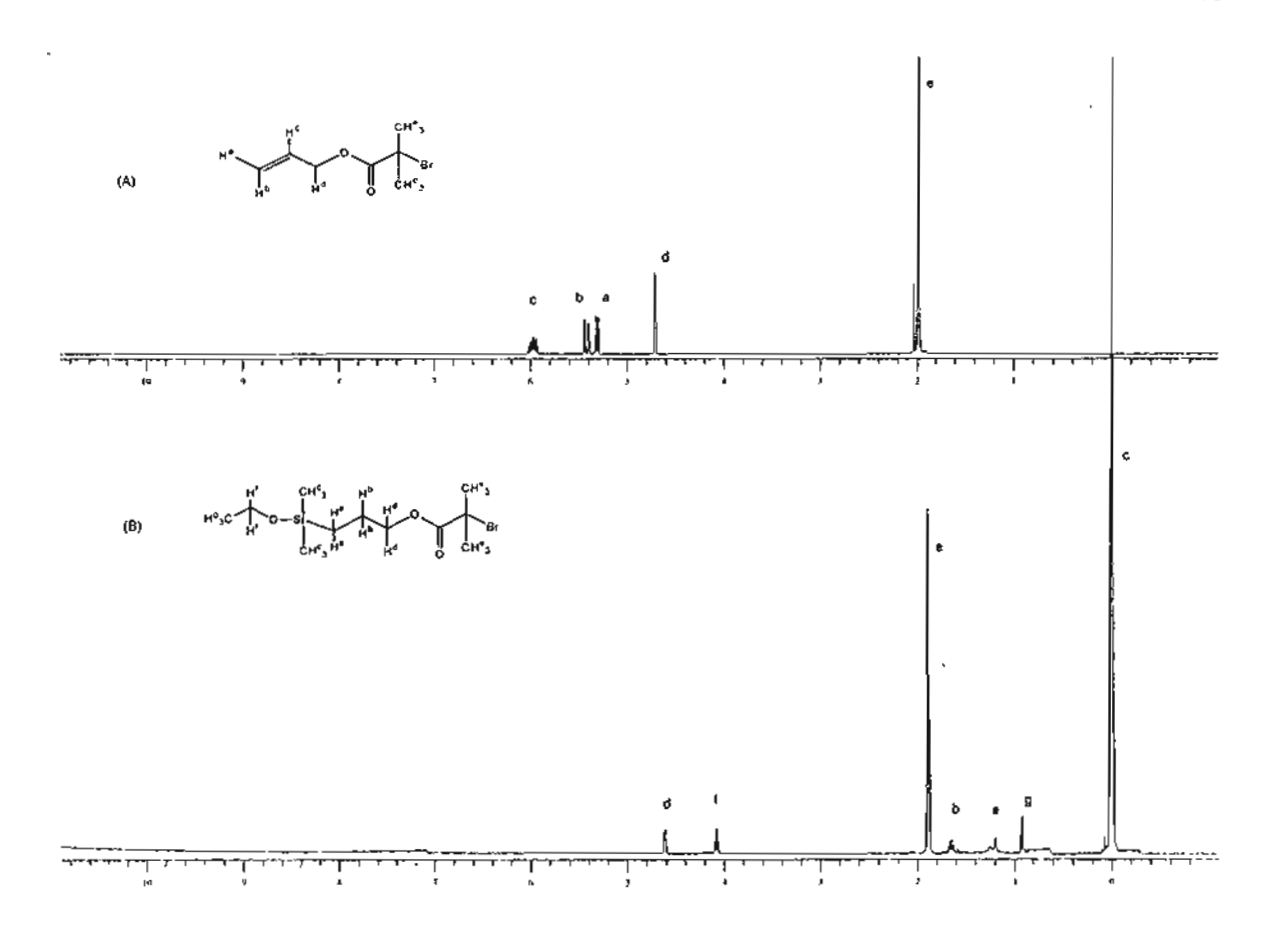


**Figure 4.1** <sup>1</sup>H NMR spectra of (A) prop-2'-enyl-2-bromoisobutyrate and (B) 3-(dimethylethoxysilyl)propyl-2-bromoisobutyrate

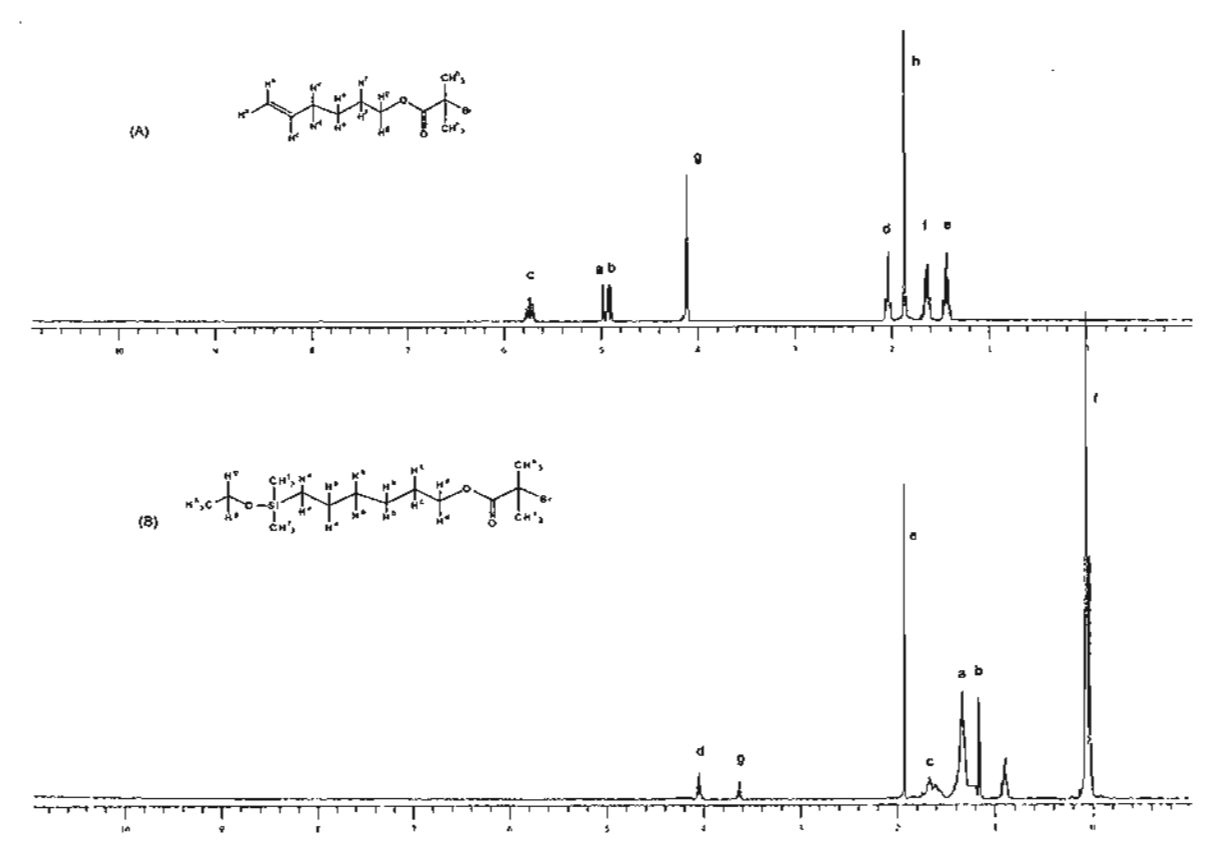


Figure 4.2 <sup>1</sup>H NMR spectra of (A) hex-5-enyl-2-bromoisobutyrate and (B) 6-(dimethylethoxysilyt)hexyl-2-bromoisobutyrate

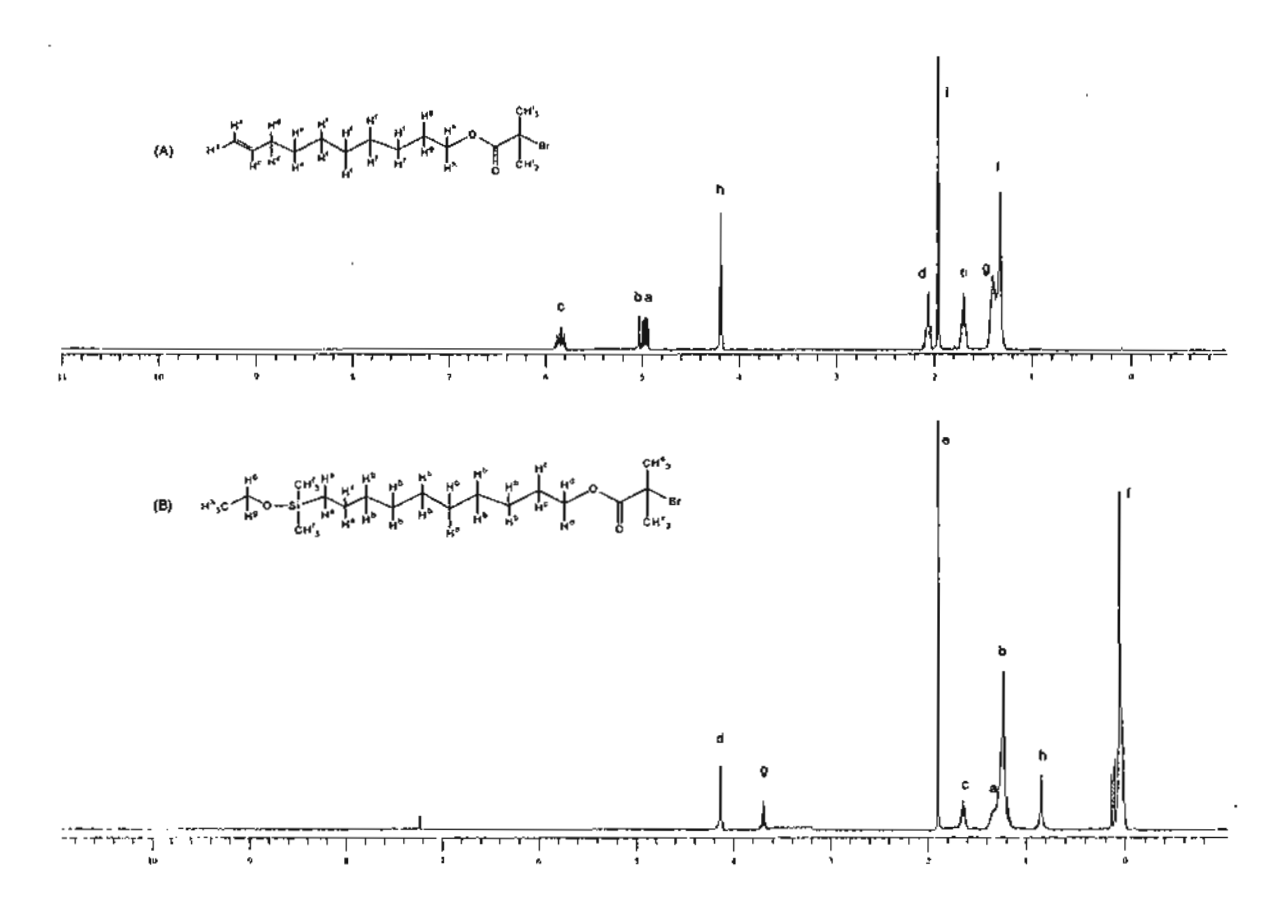


Figure 4.3 <sup>1</sup>H NMR spectra of (A) dec-9-enyl-2-bromoisobutyrate and (B) 10-(dimethylethoxysilyl)decyl-2-bromoisobutyrate

### 4.1.3 Synthesis of Propyl-2-bromoisobutyrate as a "Sacrificial" Initiator

7

The nucleophilic substitution of 1-propanol with 2-bromoisobutyryl bromide in tetrahydrofuran gave propyl-2-bromoisobutyrate (7) as a pale yellow viscous liquid (90 %yield), which was sufficiently pure for the next synthesis without further purification after the work-up process. The <sup>1</sup>H-NMR (Figure 4.4) of product 7 showed a singlet signal of the methyl proton

from  $C(C\underline{H}_3)_2$  at 1.96 ppm indicating the success of reaction. This product was used as an "added" or "sacrificial" initiator for the polymerization of polymer brushes.

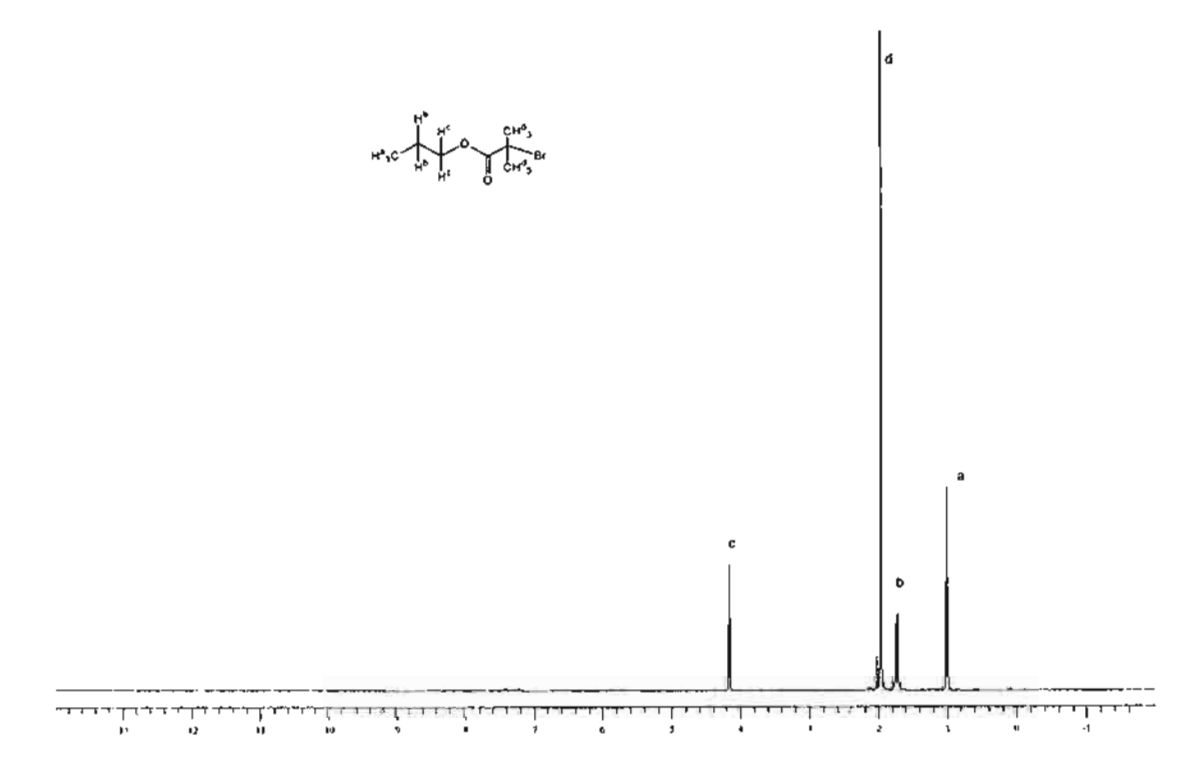


Figure 4.4 <sup>1</sup>H NMR spectrum of propyl-2-bromoisobutyrate

### 4.2 Preparation of Silicon -supported Mixed Tris(TMS)/silanol Monolayer

8

. Monolayer of tris(trimethylsiloxy) silył (tris(TMS)) was prepared by a reaction between tris(trimethylsiloxy)chlorosilane (tris(TMSCI)) and silanol groups on silicon substrate. By

controlling the kinetics of this reaction, a series of mixed monolayer of tris(TMS)/silanot having different surface coverage of tris(TMS) can be prepared. The kinetics of reaction can be monitored by ellipsometry and contact angle analysis. As shown in Figure 4.5, the ellipsometric thickness of tris(TMS) layer slowly increased as a function of reaction time and reached its maximum of ~ 20 Å after 4 days. Water contact angle data are shown in Figure 4.6. Initially there was a rapid rise in contact angle from 29°/15° of the cleaned silicon surface to 60°/43° within 12 h, followed by a gradual increase over a period of 1-4 days, indicating that the surface became more hydrophobic as the tris-TMS coverage was increased. The contact angle of 92°/82° was eventually obtained after 4 days of reaction.

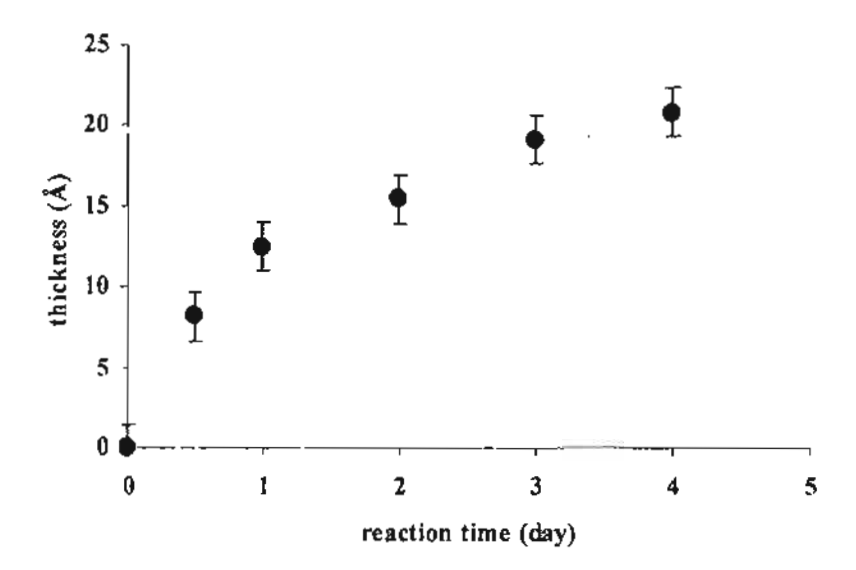


Figure 4.5 Ellipsometric thickness of tris(TMS) monolayer as a function of reaction time

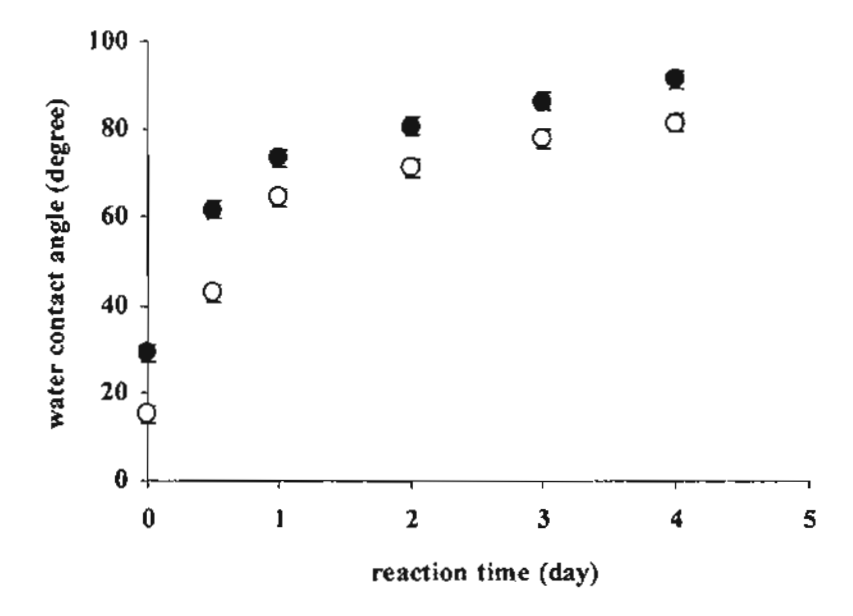


Figure 4.6 Water contact angle of tris(TMS) monolayer as a function of reaction time: advancing angle (•) and receding angle (O)

The degree of tris(TMS) coverage was determined from contact angle data according to the method proposed by Israelachvili and Gee for molecularly mixed heterogeneous surfaces. [86] The observed contact angle,  $\theta_{obs}$ , can be described in terms of the mole fractions of each component,  $f_1$  and  $f_2$ , as well as the contact angles for the pure surface of each component,  $\theta_1$  and  $\theta_2$ , by

$$[1 + \cos\theta_{obs}]^2 = f_1 [1 + \cos\theta_1]^2 + f_2 [1 + \cos\theta_2]^2$$
 (4.1)

$$f_1 + f_2 = 1 (4.2)$$

when

 $\theta_{obs}$  = the observed advancing angle of tris(TMS) coverages

 $\theta_I$  = the advancing angle of complete coverage of tris(TMS) monolayers ( $\theta_I$  = 108°)

 $\theta_2$  = advancing angle of silanol monolayer ( $\theta_2 = 0^{\circ}$ )

f, = mole fractions of tris(TMS) on the surface

f2 = mole fractions of silanol groups on the surface

In this study, the surface was treated as a mixture of tris(TMS) groups ( $\theta_I = 108^{\circ}$ ) and sitanot groups ( $\theta_2 = 0^{\circ}$ ). It should be noted that the advancing contact angles were used for  $\theta_{obs}$ . In addition, the chemical composition of the tris(TMS) monolayer was determined by XPS. The data are shown in Table 4.3 along with calculated tris(TMS). The carbon content obviously increases as a function of reaction time in all cases reflecting the higher degree of tris(TMS) coverage.

Table 4.3 XPS data (15° take-off angle), water contact angle and calculated % coverage of tris(TMS) monolayer as a function of reaction time

Sample surface	XPS atomic concentration (%)			% tris(TMS)	Water contact
	Si	0	С	coverage	angle $(\theta_{\text{A}}/\theta_{\text{R}})$
silicon	40.50	29.75	29.75	0	29°/15°
tris(TMS) ,0.5 day	-		-	51	62°/43°
tris(TMS),1 day	33.66	23.26	43.08	66	73°/65°
tris(TMS) ,2 days	32.96	21.25	45.79	75	81°/71°
tris(TMS) ,3 days	31.29	21.39	47.32	82	86°/78°
tris(TMS) ,4 days	-	-	-	87	92°/82°

Our results are in good agreement with what previously reported by McCarthy and coworkers. As a result of bulky tris(TMS) groups, the reaction reaches its maximum extent as soon as the area occupied by unreacted silanol groups is too small for tris(TMSCI). Such assumption can be supported by the fact that the contact angle tends to level off after a certain period of time (3-4 days). These residual silanol groups, not blocked by tris(TMS), are reactive sites available for adsorption or chemical reaction. McCarthy and coworkers have also demonstrated that the nanoscaled holes (nanopores) in tris(TMS) monolayer (Figure 4.7) containing unreacted silanol groups can further react with smaller silanizing reagents as well as end-functionalized polystyrene to yield binary surface mixtures. [79-80] In our case, the unreacted silanol groups in the binary monolayer mixture of tris(TMS)/silanol was allowed to react with silane compounds having  $\alpha$ -bromoisobutyrate groups. The resulting binary

monolayer mixture of tris(TMS)/Qt-bromoisobutyrate was then used as a template for surface-initiated polymerization of MPC. Detail investigation is available in the following sections.

Figure 4.7 Schematic representation of nanopores in tris(TMS) monolayer

### 4.3 Preparation of Silicon-supported C-Bromoisobutyrate Monolayer

$$\begin{array}{c|cccc}
\hline
OH & + C_2H_5O - Si & O & CH_3 & O & CH_3 \\
\hline
CH_3 & C - Br & CH_3 & CH_3 & CH_3 & CH_3 & CH_3 & CH_3
\end{array}$$
silicon oxide
$$\begin{array}{c|ccccc}
CH_3 & CH_3
\end{array}$$

$$\begin{array}{c|ccccc}
CH_3 & CH_3 & CH_3 & CH_3 & CH_3 & CH_3 & CH_3
\end{array}$$
oz-bromoisobutyrate monolayer

4

Formation of PMPC brushes on silicon-supported ∞-bromoisobutyrate monolayer (homogeneous substrate) was carried out in order to determine how to control the growth of PMPC brushes. Such substrate was prepared by a reaction between silicon oxide with 3-(dimethylethoxysilyl)propyl-2-bromoisobutyrate (4). Contact angle measurements and ellipsometry were used as tools to determine an appropriate reaction time that results in the maximum graft density of initiator. Water contact angle data shown in Figure 4.8 suggest that hydrophobization has reached its maximum within 6-12 h of reaction. Water contact angle increased from 34°/15° of the cleaned silicon oxide to 71°/62° of the silicon oxide containing α-bromoisobutyrate groups. According to the result from ellipsometric analysis (Figure 4.9), a monolayer of α-bromoisobutyrate initiator was readily formed with a thickness of ~10 Å on the top of the silicon oxide layer (~34 Å) within 18-24 h.

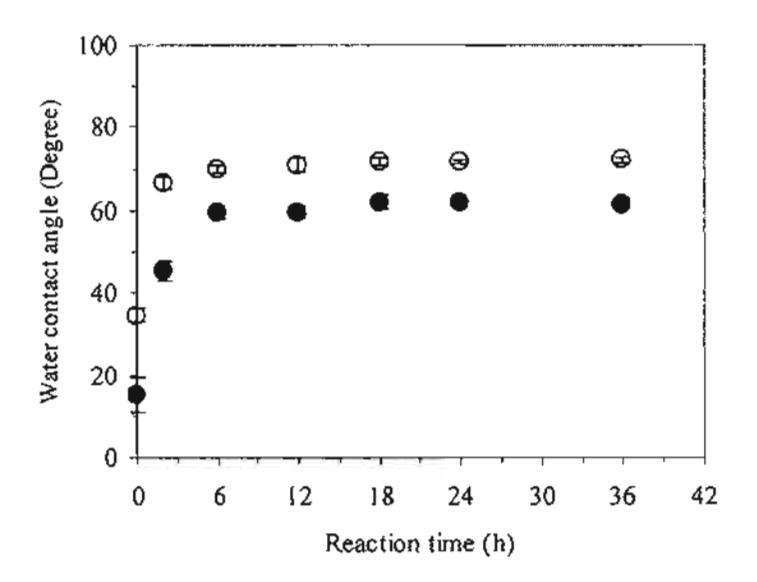


Figure 4.8 Advancing (○) and receding (●) water contact angle data of silicon oxide surface after a reaction with 4 as a function of reaction time

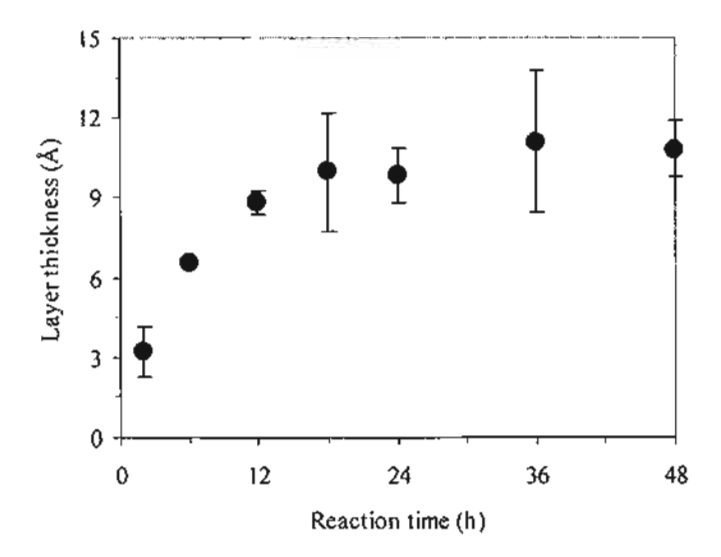


Figure 4.9 Ellipsometric thickness of the surface grafted  $\alpha$ -bromoester initiator as a function of reaction time

### 

tris(TMS) / 2-bromoisobutyrate mixed surface

Silicon-supported mixed tris(TMS)/C-bromoisobutyrate monolayers (9) were prepared by subsequent silanization of silicon-supported mixed tris(TMS)/silanol monolayer (8) having varied %tris(TMS) coverage with silane compounds having end-functionalized α-bromoisobutyrate (4, 5, 6). The silane molecules were grafted into nanopores having residual silanols in the tris(TMS) monolayers. Each silane molecule contains a bromine atom which is not present in the tris(TMS) monolayers, so the formation of silicon-supported mixed tris(TMS)/C-bromoisobutyrate monolayers can easily be assessed by XPS analysis. These data can also be used to estimate the chemical composition of binary monolayer mixtures. XPS and contact angle data for binary monolayer mixtures of tris(TMS)/C-bromoisobutyrate (n=3)

are summarized in Table 4.4. According to contact angle analysis (data are not shown), a period of 4 days was long enough for the graft density of ∞-bromoisobutyrate groups to attain its maximum value regardless of % tris(TMS) coverage.

**Table 4.4** XPS atomic composition (15° takeoff angle) and contact angle data for siliconsupported mixed tris(TMS)/∞-bromoisobutyrate (n=3) monolayer using 4 days of reaction

% tris(TMS)	XPS atomic concentration (%)				Water contact angle	
coverage	Si	0	С	Br	C : Br	$(\theta_A/\theta_R)$
0	19.37	31.24	48.52	0.87	55.8	72 <sup>°</sup> /68 <sup>°</sup>
66	39.39	34.25	25.87	0.39	66.3	73 <sup>°</sup> /52 <sup>°</sup>
75	39.97	32.84	26.82	0.37	72.5	75 <sup>°</sup> /55 <sup>°</sup>
82	37.66	27.31	34.57	0.46	75.2	80°/63°

As expected, the data indicated that the ratio of C:Br increased as the amount of tris(TMS) coverage increased. In another word, there were fewer  $\infty$ -bromoisobutyrate groups available for initiating ATRP of MPC when the content of tris(TMS) on the surface was increased. Therefore, one can use these binary monolayer mixtures of tris(TMS)/ $\infty$ -bromoisobutyrate as templates for controlling graft density of polymer brushes. Evidently, water contact angles of silicon-supported mixed tris(TMS)/ $\infty$ -bromoisobutyrate monolayer was raised as a function of %tris(TMS) coverage similar to what previously observed in the case of silicon-supported mixed tris(TMS)/silanol monolayer.

# 4.5 Surface-initiated Polymerization of MPC from Silicon-supported α-Bromoisobutyrate Monolayer

#### 4.5.1 Synthesis of PMPC in solution

This part of study was conducted with an objective to determine the effect of solvent polarity on the rate of monomer conversion in solution in order to find the most efficient solvent for polymer brush formation. We hypothesized that the length or the molecular weight of polymer brush should be linearly dependent on the monomer conversion and the molecular weight of polymer in solution. Polymerization of MPC was carried out in solution using methoxy-capped oligo(ethylene glycol)-2-bromoisobutyrate (OEGBr) as an initiator in the presence of CuBr/bpy. Polymerization was carried out at room temperature. %Conversion of MPC monomer was calculated from the ratio between  $^1$ H-NMR peak at 0.96 ppm corresponding to the  $\alpha$ -methyl proton ( $\alpha$ -CH<sub>3</sub>) of PMPC and  $^1$ H-NMR peak at 1.80 ppm corresponding to the  $\alpha$ -methyl proton ( $\alpha$ -CH<sub>3</sub>) of MPC monomer. The  $^1$ H-NMR spectra of MPC and PMPC mixed with the unreacted MPC synthesized by ATRP using [OEGBr]:[MPC] = 1:20 (a fixed target DP<sub>n</sub> of 20 ( $\overline{M}_n$  = 6,000)), are shown in Figure 4.10.

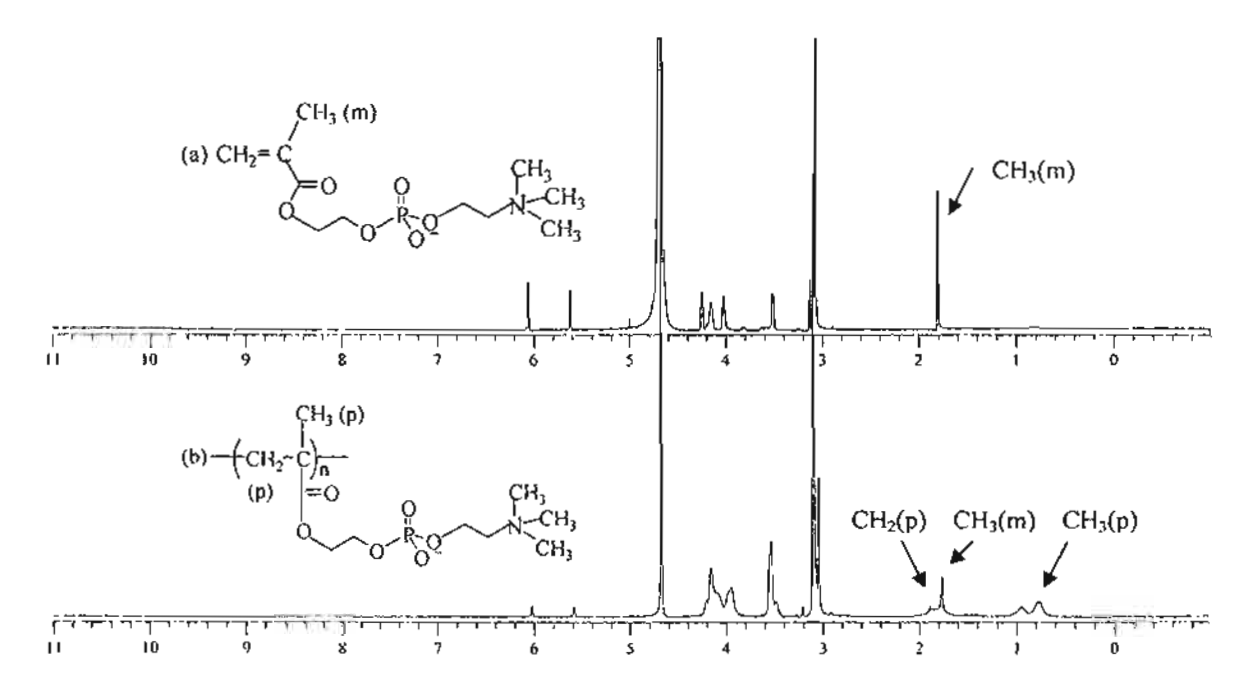


Figure 4.10 <sup>1</sup>H NMR spectra of (a) MPC and (b) PMPC mixed with the unreacted MPC synthesized by ATRP using {OEGBr]:{MPC} = 1:20.

Polymerization was carried out in water, methanol:water = 1:1 (v/v) and 4:1 (v/v). The rate of monomer conversion was followed by analyzing the solution withdrawn from the mixture during polymerization. The results shown in Figure 4.11 suggested that the rate of monomer conversion increased as the polarity of solvent increased. The polymerization in aqueous has reached almost 100% conversion within 150 min of reaction. The rate of monomer conversion was significantly reduced in the presence of methanol which is a less polar solvent in comparison with water. These results agree very well with the previous data reported by Armes and coworkers [40]. They explained that MPC can be polymerized to high conversion in both water and methanol at ambient temperature via atom transfer radical polymerization (ATRP). The narrow polydispersities ( $\overline{M} \downarrow \overline{M}_n = 1.15-1.35$ ) were obtained in both aqueous and alcoholic media at 20°C. However, slower polymerizations and narrower polydispersities were always obtained in alcoholic solution, and chain extension experiments indicated significantly greater living character under these conditions. Moreover, these results support that the Cu(I)Br/bpy complexes can well solvate in polar solvent [17]. Nanda and Matyjaszewski studied the effect of polarity of the medium on the activation rate constants ( $k_{\rm act}$ ) in atom transfer radical polymerization. They found the kact was larger in more polar solvents compared to less polar solvent because of the effect of [CuBr]/[bpy] complex. In more polar media, the bromide anion is sufficiently stable and well solvated, resulting in Cu(bpy)2 Br species. However, in less polar media, Br is destabilized and concurrently binds much stronger to Cu(I)Br than bpy does, resulting in Cu(bpy)2 CuBr2 species. However, there are data suggest that the aqueous ATRP of MPC has less than ideal living character [40]. Armes and coworkers believe that aqueous ATRP is not well-suited for synthesis of controlled-structure block copolymer. There are two plausible explanations for the reduced living character encountered in aqueous ATRP syntheses. First, the copper-halogen bond of the Cu(II) complex is likely to be less covalent (more ionic) in aqueous media, which could reduce the efficiency of polymer radical deactivation. Second, the terminal halogen atom on the polymer chain ends may be prone to hydrolysis.

Even though PMPC brushes grew more rapidly in a more polar aqueous media in comparison with a less polar alcoholic media in the absence of "added" initiator, water seems to deteriorate the livingness of reaction. For this reason, two less polar solvent systems were selected in this study: mixed methanol:water = 4:1 (v/v) and pure methanol.

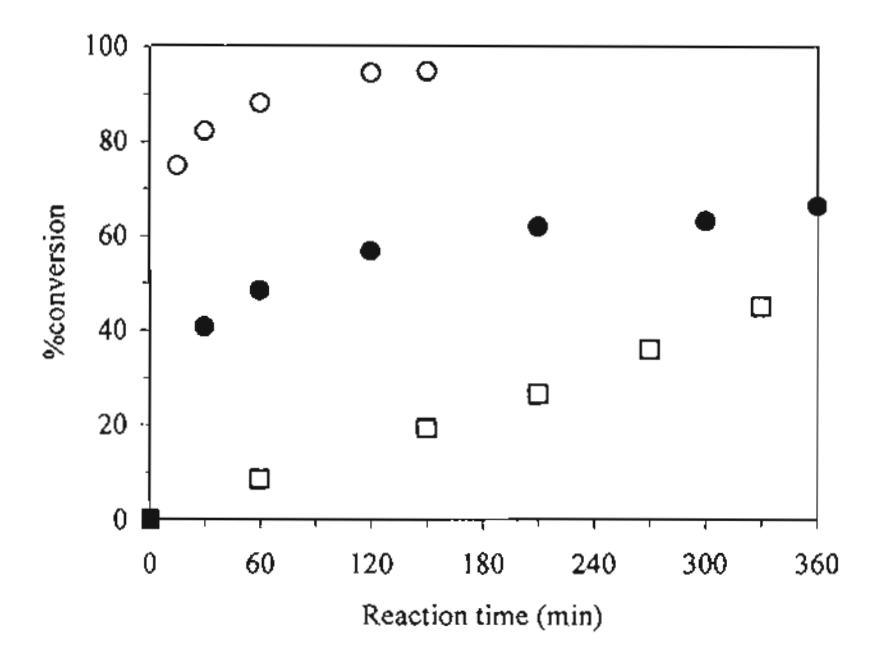


Figure 4.11 %Monomer conversion as a function of reaction time using water (O), methanol:water = 1:1 (v/v) ( $\blacksquare$ ), and 4:1 (v/v) ( $\square$ ) as a solvent

Sections 4.5.2 and 4.5.3 focus on two experimental parameters that would affect the efficiency of PMPC brush growth: (1) "sacrificial" or "added" initiator and (2) deactivator. The word "sacrificial" initiator or "added" initiator represents free initiator which is not attached to the surface. It was intentionally added in the solution during surface-initiated polymerization due to 2 major reasons. The first reason is to use this free initiator (propyl-2-bromoisobutyrate in this case) to simultaneously initiate polymerization in the solution. Previous work reported by Fukuda has demonstrated that the molecular weight of this "free" polymer formed in the solution closely resembled that of the grafted polymer brushes cleaved from the surface. Thus, it can be used to monitor the surface-grafted polymerization process.[81] The free initiator plays a role not only as an indicator of the polymerization but also as a controller for the ATRP on the surface. The second reason has a lot to do with the activation/deactivation cycles of ATRP process (Scheme 4.2). In the polymerization without an "added" initiator, the concentration of the Cu complex (deactivator) produced from the reaction at the substrate surface is too low to reversibly deactivate polymer radicals with a sufficiently high rate. In the presence of an "added" initiator, the deactivator was generated by radical termination in the initial stage of

polymerization until a nearly steady state concentration of copper (II) (Cu<sup>II</sup>) was achieved. The "added" initiator would help increasing and adjusting the concentration of the Cu<sup>II</sup> complex as in a free ATRP system. The adjustment of the Cu<sup>II</sup> concentration could be made by directly adding an appropriate amount of the Cu<sup>II</sup> complex which acts as a deactivator.

$$P_m = X + Cu(I)X / Ligand$$

$$\begin{array}{c} k_{act} \\ \hline k_{deact} \\ \hline k_p \\ \end{array} + X - Cu(II)X / Ligand$$

$$\begin{array}{c} k_1 \\ \hline k_1 \\ \hline \end{array}$$

$$\begin{array}{c} P_m = P_n \\ \hline \end{array}$$
Termination

Scheme 4.2 The activation/deactivation cycles of ATRP process

#### 4.5.2 PMPC brushes prepared in the presence of "added" initiator

Figure 4.12 shows the development of PMPC thickness as a function of time at two targeted degrees of polymerization (DP) using mixed methanol:water = 4:1 (v/v) as a solvent. The mole ratio of added initiator:CuBr;bpy of 1:1:2 was fixed while two mole ratios of MPC:added initiator of 50:1 and 200:1 were used. The thickness of PMPC layer increased with the increase of targeted DP. For both targeted DPs, the thickness increased linearly with time at the beginning. The rate of thickness increase of PMPC brushes seems to slow down at the later stage. This was probably due to loss of active chain ends by termination and/or diffusion limitations of monomer to the surface. This result clearly indicated that both polymerization time and [MPC]:[added initiator] ratio can be used as tools for controlling the growth of polymer brushes. The linear increase of thickness as a function of polymerization time evidently suggests that the polymerization is living in character.

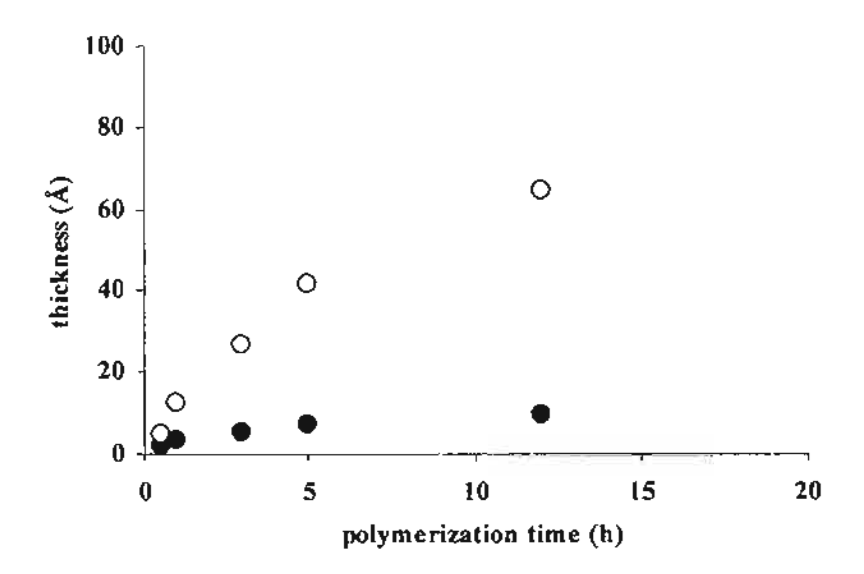


Figure 4.12 Ellipsometric thickness of PMPC brushes versus polymerization time in the presence of "added" initiator, [MPC]:[added initiator] = 200:1 (○) and [MPC]:[added initiator] = 50:1(●) using methanol:water = 4 : 1 (v/v) as a solvent

Under the same condition to obtain targeted DP of 200, PMPC brushes prepared in pure methanol was relatively thinner than those prepared in mixed methanol/water. The relationships between PMPC brush thickness prepared in pure methanol and the one prepared in mixed methanol/water and reaction time are shown in Figure 4.13. These results agree well with the data reported by Armes and coworkers which was previously discussed in section 4.5.1. In spite of the variation in thickness of PMPC brushes, good control over the growth PMPC brushes can be achieved using both mixed methanol:water (4:1 v/v) and pure methanol.

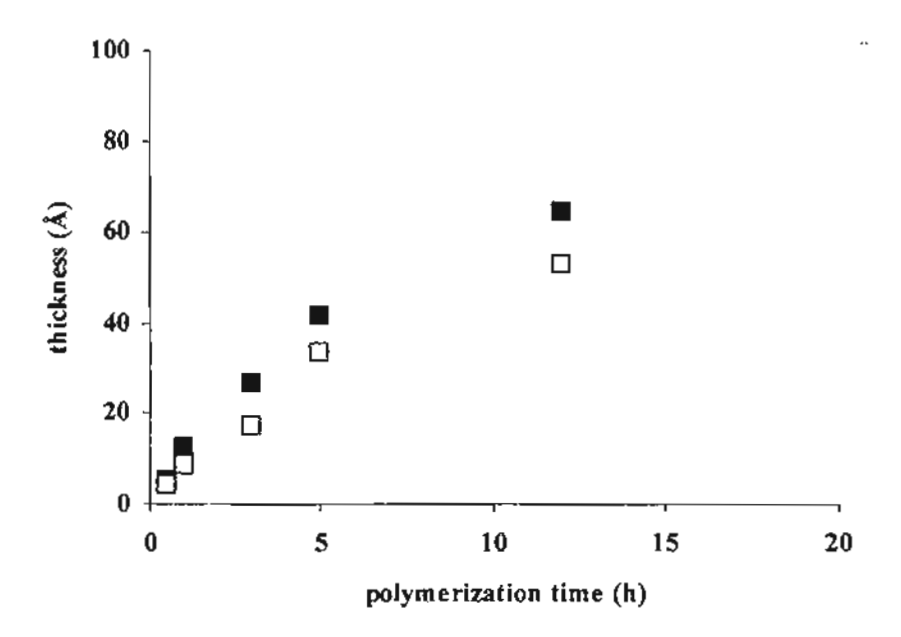


Figure 4.13 Ellipsometric thickness of PMPC brushes versus polymerization time for targeted DP = 200 in methanol:water = 4 : 1 (v/v) (■) and pure methanol (□)

The growth of PMPC brushes can also be monitored by water contact angle analysis. Figure 4.14 shows advancing  $(\theta_A)$  and receding  $(\theta_R)$  water contact angles of silicon-supported PMPC brushes as a function of polymerization time. Both advancing and receding contact angles rapidly dropped with time from  $72^{\circ}/68^{\circ}$  of hydrophobic silicon-supported  $\alpha$ -bromoisobutyrate monolayer (n = 3) to  $\sim 20^{\circ}/1^{\circ}$  of hydrophilic silicon-supported PMPC brushes after 1 h of reaction. The contact angle data also imply that the surface bearing PMPC brushes is quite homogeneous and smooth. The independence of water contact angle on the thickness of PMPC brushes evidently suggests that the growing of each polymer brush is simultaneous and living in character.

The receding angle was re-plotted together with ellipsometric thickness of PMPC brushes (Figure 4.15) in order to demonstrate that the wetting has reached its equilibrium at relatively low thickness (~10 Å). Despite the slightly thinner layer of PMPC brushes, a similar trend was also observed in Figure 4.16 when pure methanol was used as a solvent.

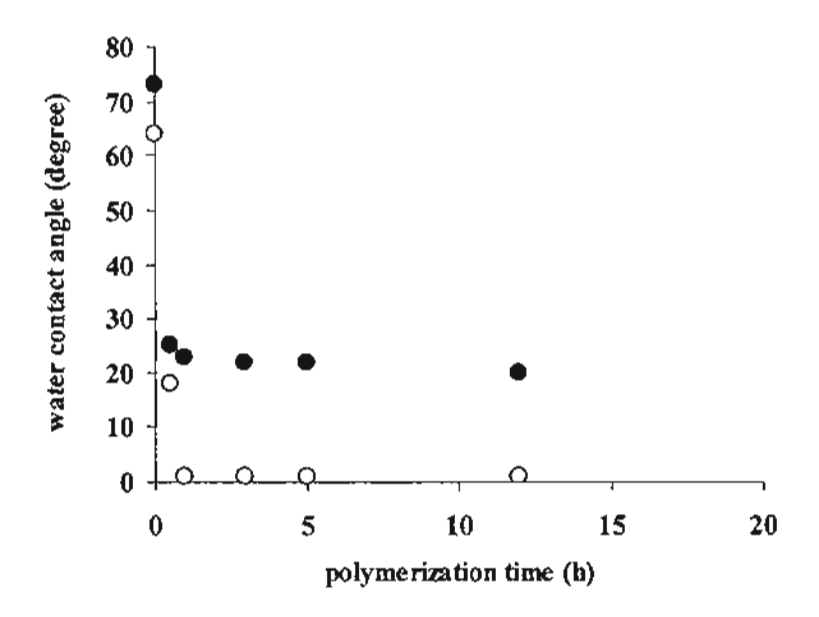


Figure 4.14 Water contact angle data of PMPC brushes versus polymerization time for targeted DP = 200 using methanol/water = 4:1 (v/v) as a solvent:  $\theta_A$  ( $\bullet$ ) and  $\theta_R$  ( $\circ$ ).

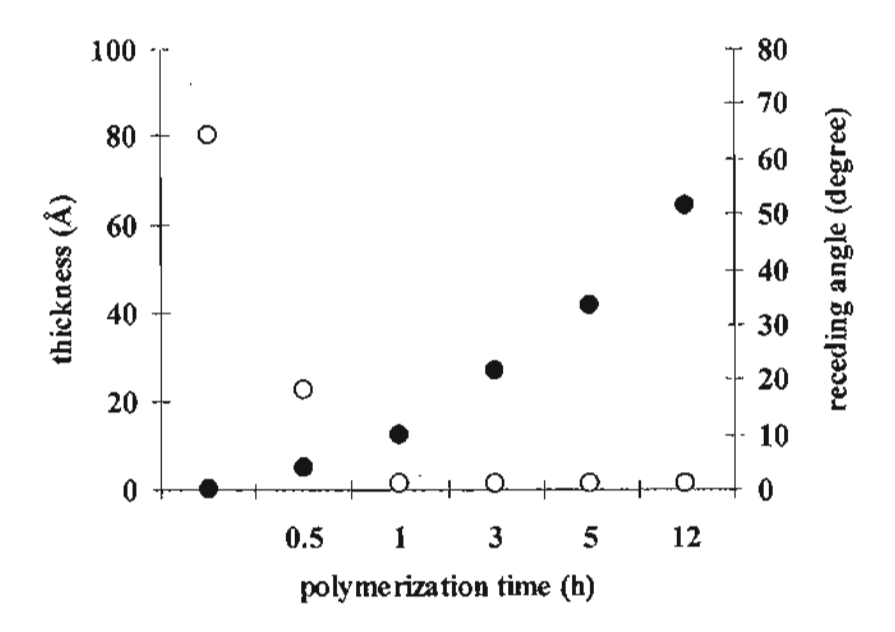


Figure 4.15 Ellipsometric thickness ( $\bullet$ ) and receding water contact angle ( $\theta_R$ ) (O) of PMPC brushes versus polymerization time for targeted DP = 200 using methanol:water = 4:1 (v/v) as a solvent

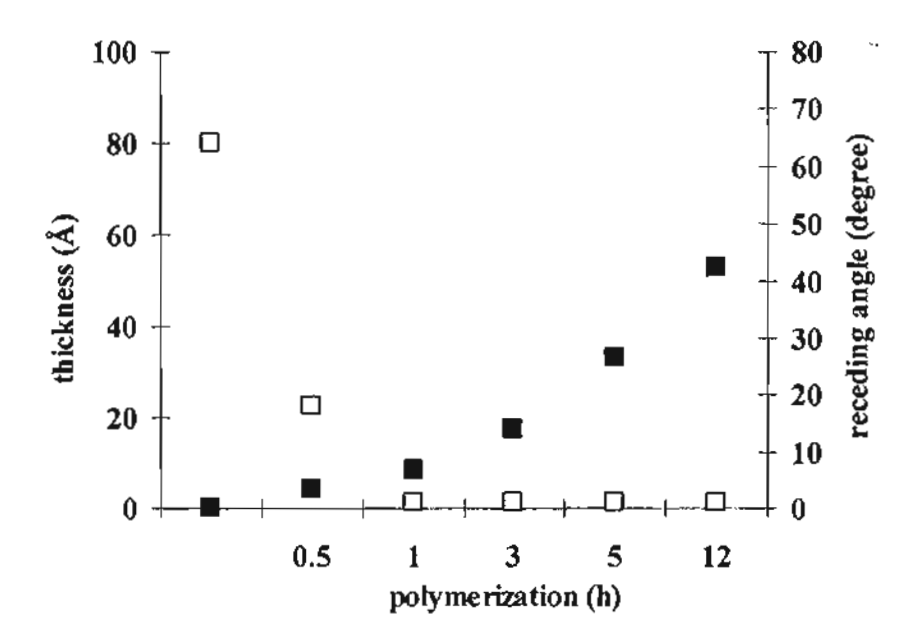


Figure 4.16 Ellipsometric thickness ( $\blacksquare$ ) and receding water contact angle ( $\theta_R$ ) ( $\square$ ) of PMPC brushes versus polymerization time for targeted DP = 200 using methanol as a solvent

# 4.5.3 PMPC brushes prepared in the presence of deactivator

Although the addition of "added" initiator is strongly recommended by many research groups as an effective method to control the growth of polymer brushes, some of them have argued that such method generates a large quantity of free polymer formed in the solution. This free polymer as a side product of polymer brush formation somewhat leads to the tedious process of surface cleaning after reaction.

To overcome these disadvantages, an alternative approach of adding an deactivator has been proposed. In this research, CuBr<sub>2</sub> was added in the solution to generate Cu(II) which can act as the deactivator in the absence of "added" initiator. Figure 4.17 illustrates the development of thickness of PMPC brushes using different mole ratio of CuBr:CuBr<sub>2</sub> (1:0, 1:0.1 and 1:0.5) and [MPC] = 0.012 mole. In the absence of CuBr<sub>2</sub>, the thickness increased rapidly in the early stage and level off after a certain period of time indicating that the polymerization was not well controlled. This can be explained by the fact that the concentration of the Cu<sup>II</sup> complex (deactivator) produced from the reaction at the substrate surface is too low to reversibly deactivate polymer radicals with a sufficiently high rate. The radicals on the surface

once generated could not easily revert with the dormant state, and thus participated in side reactions leading to the loss of active chains. The major side reaction on the surface was bimotecular termination. Adding 10 mol% CuBr<sub>2</sub> (CuBr:CuBr<sub>2</sub> =1:0.1) to the system decreased the initial polymerization rate. The reduced rate was caused by lower radical concentration on the surface due to the added CuBr<sub>2</sub> that deactivated the radicals. The thickness of PMPC brushes linearly increased as a function of polymerization time suggesting that polymerization is living and can be better controlled. Increasing the CuBr<sub>2</sub> concentration to 50 mol% (CuBr:CuBr<sub>2</sub> =1:0.5) minimized side reactions of the radicals at the surface, but decreased the rate of polymerization significantly.

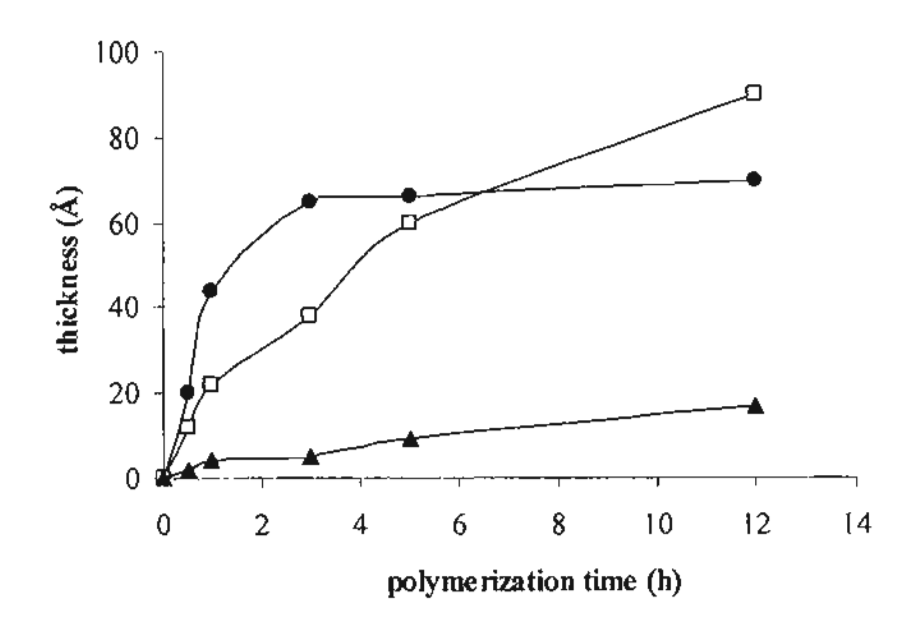


Figure 4.17 Ellipsometric thickness of PMPC brushes versus polymerization time for different [CuBr]/[CuBr<sub>2</sub>] ratios at targeted DP of 200 using methanol:water = 4:1 (v/v) as a solvent: [CuBr]/[CuBr<sub>2</sub>] = 1:0 ( $\bullet$ ), 1:0.1 ( $\Box$ ) and 1:0.5 ( $\triangle$ )

#### 4.5.4 Molecular weight and graft density of PMPC brushes

It is rather difficult to obtain the molecular weight of the polymer brush directly since the amount of polymer on the silicon wafer is too small to degraft and analyze. The information related to molecular weight distribution and molecular weight which can be used to calculate the graft density of polymer brushes can thus be obtained from the "free" polymer chains formed by the "added" initiator in solution. Figure 4.18 illustrates the change in the molecular

weight  $(\overline{M}_n)$  and molecular weight distribution  $(\overline{M}_n)$  of free PMPC produced in methanol:water = 4:1 (v/v) as a function of polymerization time. The molecular weight increased linearly with increasing polymerization time. The molecular weight distribution being close to 1.0 suggested that polymerization mechanism is living.

Figures 4.19 and 4.20 show ellipsometric thicknesses of grafted PMPC brushes versus the molecular weight ( $\overline{M}_n$ ) of PMPC formed in solution that were produced by the free initiator. Linear relationships were observed for both targeted DPs, demonstrating a good control of the grafting process with the added free initiator. The thicknesses at the targeted DP = 200 were almost a factor of four greater than those at the targeted DP = 50.

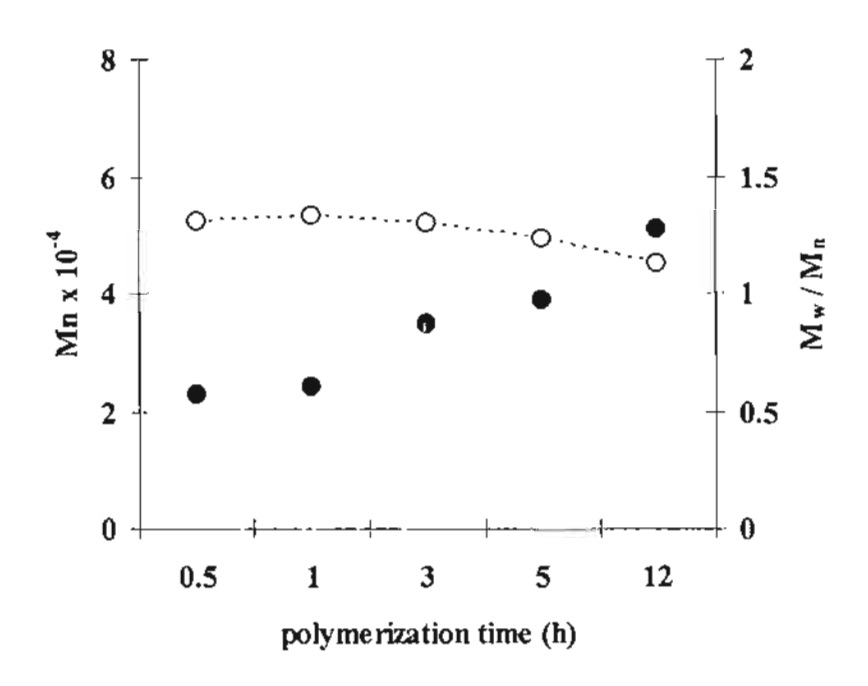


Figure 4.18 Molecular weight  $(\overline{M}_n)$  ( $\bullet$ ) and molecular weight distribution  $(\overline{M}_w/\overline{M}_n)$  (O) of free PMPC for targeted DP = 200 produced in methanot:water = 4:1 (v/v) as a function of polymerization time

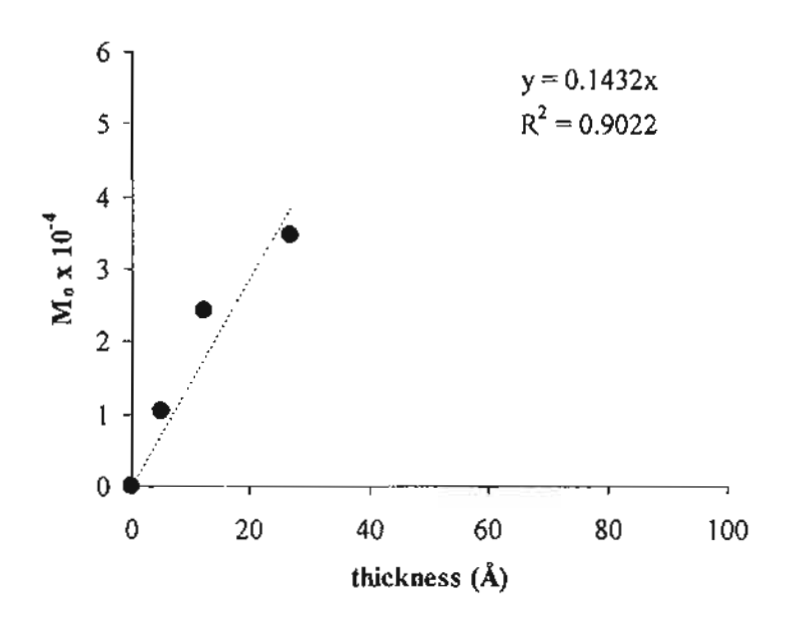


Figure 4.19 Relationship between ellipsometric thickness of PMPC brushes and molecular weight ( $\overline{M}_n$ ) of free PMPC for targeted DP = 200 produced in methanol:water = 4:1 (v/v)

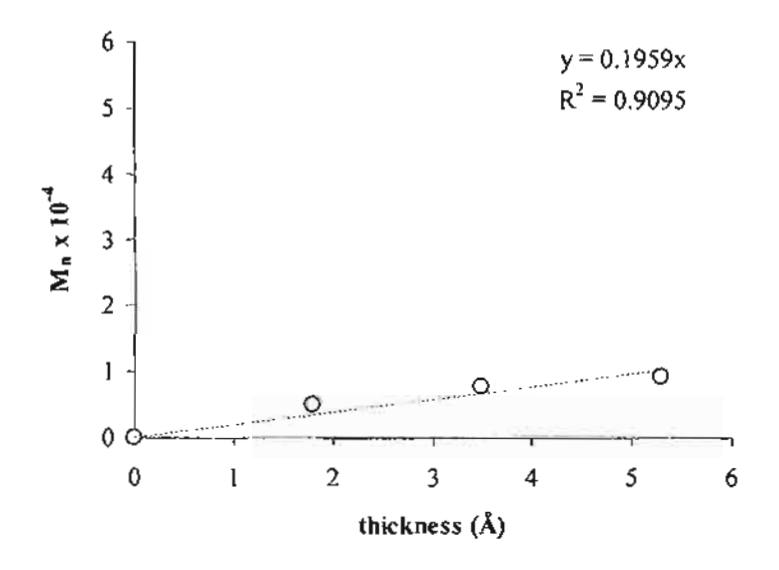


Figure 4.20 Relationship between ellipsometric thickness of PMPC brushes and molecular weight ( $\overline{M}_{\rm n}$ ) of free PMPC for targeted DP = 50 produced in methanol:water = 4:1 (v/v)

Grafting density ( $\sigma$ ) which is a unit per cross-sectional area ( $A_x$ ) per chain can be determined from the corresponding film thickness (t) and the molecular weight of the chain (M) from the following equation by

$$\sigma = \underbrace{\iota \rho \, N_A}_{A_X} = \underbrace{1}_{A_X} \tag{4.3}$$

Where  $\rho$  is the mass density (1.30 g/cm<sup>3</sup> for PMPC) and  $N_A$  is Avogadro's number. Using slopes obtained from the plots in Figure 4.19 and 4.20 which correspond to M/t, the calculated grafting densities are 0.46 and 0.34 chains/nm<sup>2</sup> for targeted DP = 200 and targeted DP = 50, respectively. These results agree quite well with the data previously reported that the graft densities for various polymers prepared by surface-initiated ATRP were also ranged from 0.1 to 0.6 chains/nm<sup>2</sup> [64]. Feng and coworkers [87] also reported grafting densities of PMPC brushes as 0.32 and 0.28 chains/nm<sup>2</sup> for the targeted DP = 200 and targeted DP = 50, respectively.

# 4.5.5 Confirmation of PMPC brushes by XPS

XPS was used to confirm the formation of the initiator monolayer and the growth of PMPC brushes. The data is outlined in Table 4.5. The  $\alpha$ -bromoisobutyrate layer was indicated by the signal of  $Br_{3d}$ . The  $N_{1s}$  and  $P_{2p}$  data suggested that phosphatidylcholine analogous groups were present on the surface after the formation of PMPC brushes. The N/P ratio at  $15^{\circ}$  of take-off angle of  $\sim$  0.8 reasonably agreed with the stoichiometric ratio of MPC unit. Due to partial x-ray damage of bromine during XPS analysis along with the fact that bromine is buried within the polymer brushes when the brushes are relatively thick [88], the percentage of  $Br_{3d}$  is neither quantitative nor consistent with the percentages of  $N_{1s}$  and  $P_{2p}$ .

**Table 4.5** XPS elemental surface composition (%) of silicon surfaces before and after the formation of PMPC brushes

Surface	Si <sub>2p</sub>	C <sub>1s</sub>	O <sub>1s</sub>	Br <sub>3d</sub>	P <sub>2p</sub>	N <sub>1s</sub>
Silicon	40.50	29.75	29.75	-	-	-
Silicon-supported α- bromoisobutyrate monolayer	19.37	48.52	31.24	0.87	-	-
Silicon-supported PMPC brushes (thickness = 64 Å)	16.52	48.97	32.38	0.00	1.16	0.96

# 4.6 Surface-initiated Polymerization of MPC from Silicon-supported Mixed Tris(TMS)/∞-Bromoisobutyrate Monolayer

As mentioned earlier, silicon-supported mixed tris(TMS)/ $\alpha$ -bromoisobutyrate monolayer was intended to be used as nanoscaled templates for the formation of PMPC brushes. In this section, the growth of PMPC brushes as a function of %tris(TMS) coverage, the type of grafted  $\alpha$ -bromoisobutyrate and polymerization time are primarily discussed in terms of water contact angle and ellipsometric thickness. The results from morphological studies of silicon-supported polymer brushes are separately provided in section 4.7.

As demonstrated in Figure 4.21, the thickness of PMPC brushes which corresponded with the density and length of polymer brushes decreased as the %tris(TMS) coverage increased. Due to the hydrophobicity of tris(TMS) groups surrounding  $\alpha$ -bromoester initiators, the growth of polymer brush is more favorable in a more surface-wettable solvent, methanol in this particular case, than water. Using 5h of polymerization, PMPC brushes prepared in methanol were relatively thicker than those obtained in water.

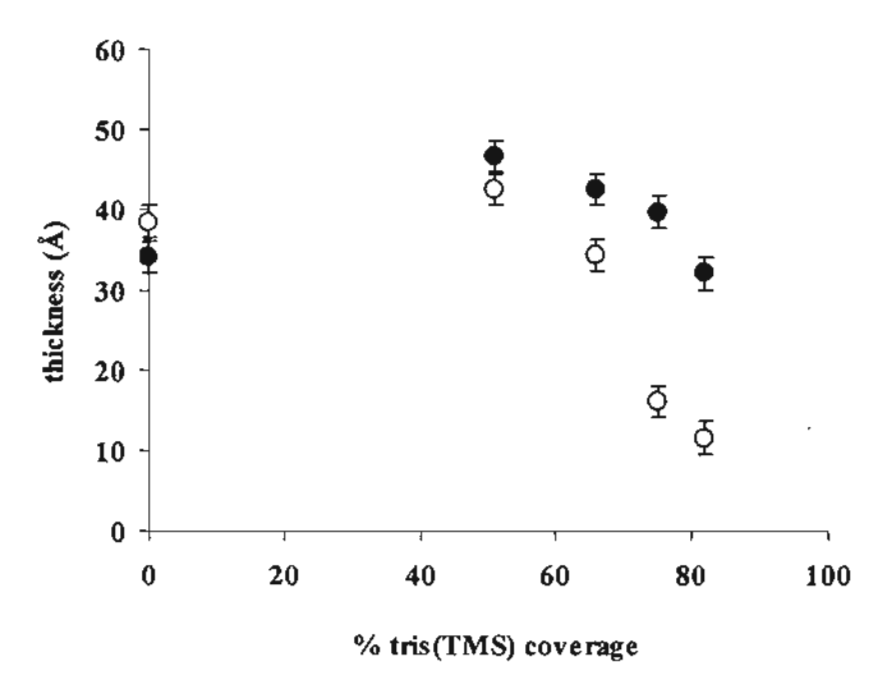


Figure 4.21 Ellipsometric thickness of PMPC brushes grown from silicon-supported mixed tris(TMS)/α-bromoisobutyrate monolayer using methanol (•) or water (O) as a solvent

As expected, the advancing and receding angle of PMPC brushes on mixed tris(TMS)/QL-bromoisobutyrate increased with increasing % tris(TMS) coverage. As shown in Figure 4.22, relatively high advancing angles reflect the assumption that tris(TMS) groups dominate at the polymer/air interfaces. Receding angles can better represent how hydrophilic the mixed surface is.

The growth of PMPC brushes from nanopores can also be tuned by polymerization time. Figure 4.23 shows the thickness and receding water contact angle of the silicon-supported tris(TMS)/PMPC brushes having 82% tris(TMS) coverage as a function of polymerization time. The longer the polymerization proceeds, the thicker the polymer brush and the more hydrophilic the surface become.

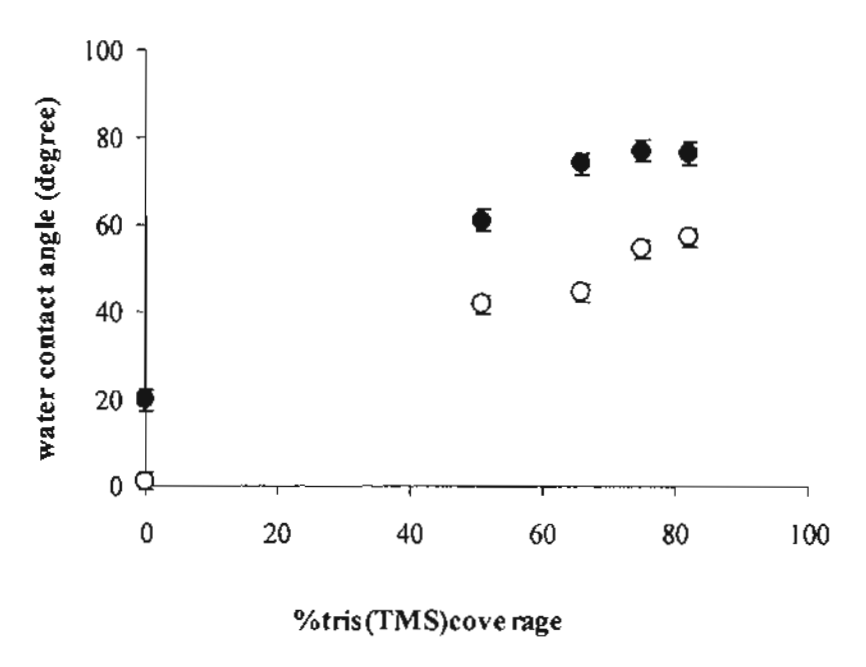


Figure 4.22 Water contact angle of PMPC brushes grown from silicon-supported mixed tris(TMS)/ $\alpha$ -bromoisobutyrate monolayer using methanol as a solvent for 5 h:  $\theta_{\rm A}$  ( $\bullet$ ) and  $\theta_{\rm R}$  ( $\circ$ )

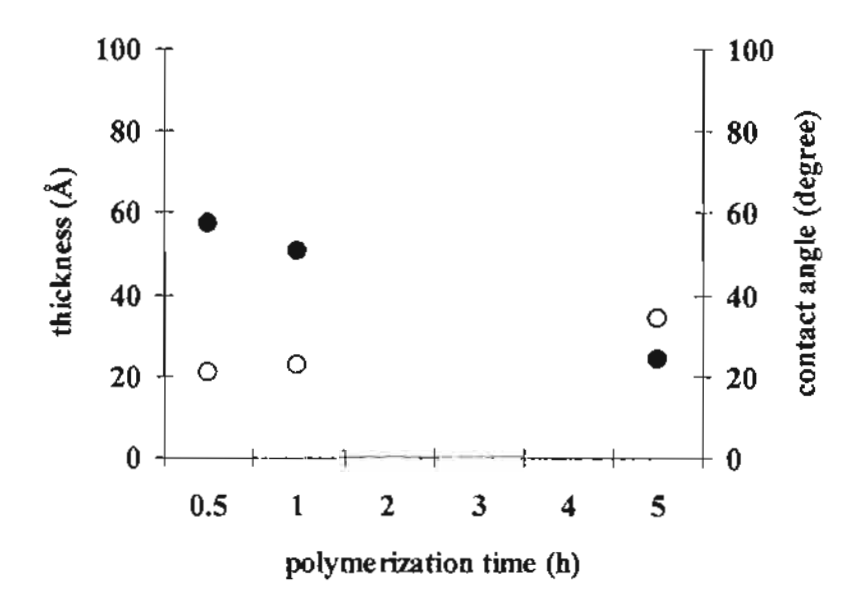


Figure 4.23 Ellipsometric thickness (•) and receding water contact angle (O) of siliconsupported mixed tris(TMS)/PMPC brushes having 82% tris(TMS) coverage as a function of polymerization time

Originally, the fact that the surface having a certain %tris(TMS) coverage (~15-20 Å) is relatively thicker than  $\alpha$ -bromoisobutyrate monolayer (~10 Å) brought a concern that the short alkyl chain, especially for the silane having n=3 might be buried in the nanopores surrounded by tris(TMS) and unable to initiate polymerization. Therefore, three analogous series of silane compounds having end-functionalized  $\alpha$ -bromoisobutyrate groups were used to react with residual silanols in nanopores in order to determine the effect of alkyl spacer (n = 3, 6, and 10) between the surface-immobilized end and the other end bearing  $\alpha$ -bromoisobutyrate group on the efficiency to initiate polymerization. The immobilized  $\alpha$ -bromoisobutyrate initiator is defined according to its alkyl spacer as n<sub>3</sub>, n<sub>6</sub>, and n<sub>10</sub> for propyl (n=3), hexyl (n=6) and decyl (n=10), respectively.

Figure 4.24 depicts the thickness of PMPC brushes grown from silicon-supported mixed tris(TMS)/ $\Omega$ -bromoisobutyrate monolayer having 82%tris(TMS) coverage. The density of surface-tethered initiator was varied a function of grafting time in the range of 1–4 days. Polymerization was then conducted in methanol using [MPC] = 0.08 M for 5 h in the presence of added initiator. Having similar graft density of initiator (using the same grafting time), the thicknesses of PMPC brushes grown from  $n_6$  and  $n_{10}$  are higher than that of PMPC brushes grown from  $n_3$ . This outcome can possibly be rationalized as the better mobility and the longer alkyl spacer of  $n_6$  and  $n_{10}$  allowing them to conquer the steric hindrance of the surrounding tris(TMS) and reach monomers more efficiently than  $n_3$ . It should be noted that the thicknesses of silicon-supported  $\Omega$ -bromoisobutyrate monolayer of  $n_6$  and  $n_{10}$  are 15 Å and 18 Å, respectively. It was also observed that the higher graft density or the longer grafting time of initiator, the denser and the thicker PMPC brushes.

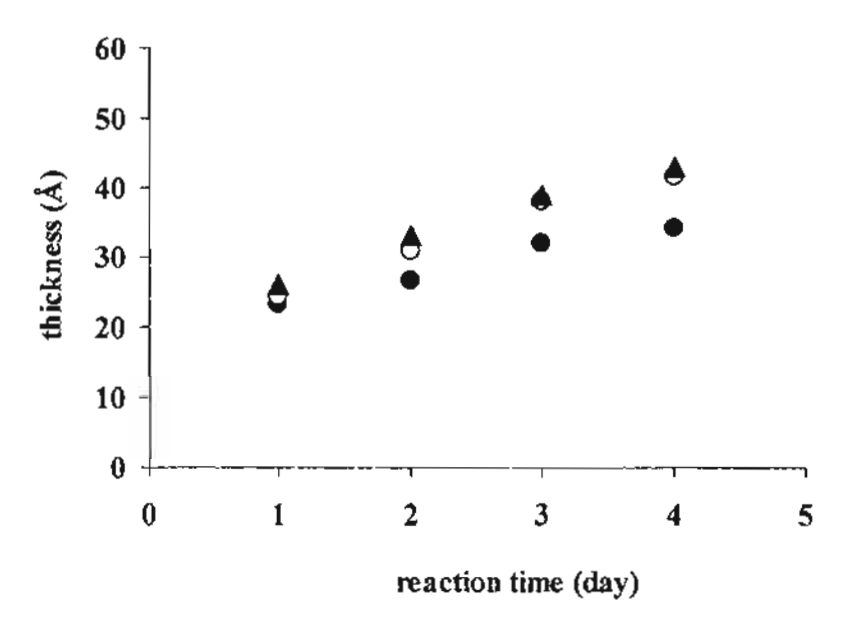


Figure 4.24 Ellipsometric thickness of PMPC brushes grown from silicon-supported mixed tris(TMS)/ $\alpha$ -bromoisobutyrate monolayer having 82% tris(TMS) coverage versus grafting time of initiator in methanol for 5 h:  $n_3$  ( $\bullet$ ),  $n_6$  ( $\bigcirc$ ) and  $n_{10}$  ( $\triangle$ )

Using the grafting time of 4 days for all three initiators, the kinetics of surface-initiated polymerization of MPC on silicon-supported mixed tris(TMS)/ $\alpha$ -bromoisobutyrate monolayer (as  $n_3$ ,  $n_6$ , and  $n_{10}$ ) having 82% tris(TMS) coverage were determined. The thickness of PMPC brushes as a function of polymerization time is illustrated in Figure 4.25. These data clearly suggested that not only does the alkyl spacer influence the ability of  $\alpha$ -bromoisobutyrate to react with monomer but also how fast it can react. The data points at 1h can distinguish the kinetics between  $n_6$ , and  $n_{10}$  at an early stage of polymerization. Nonetheless, such dissimilarity is no longer noticeable at a later stage of polymerization.

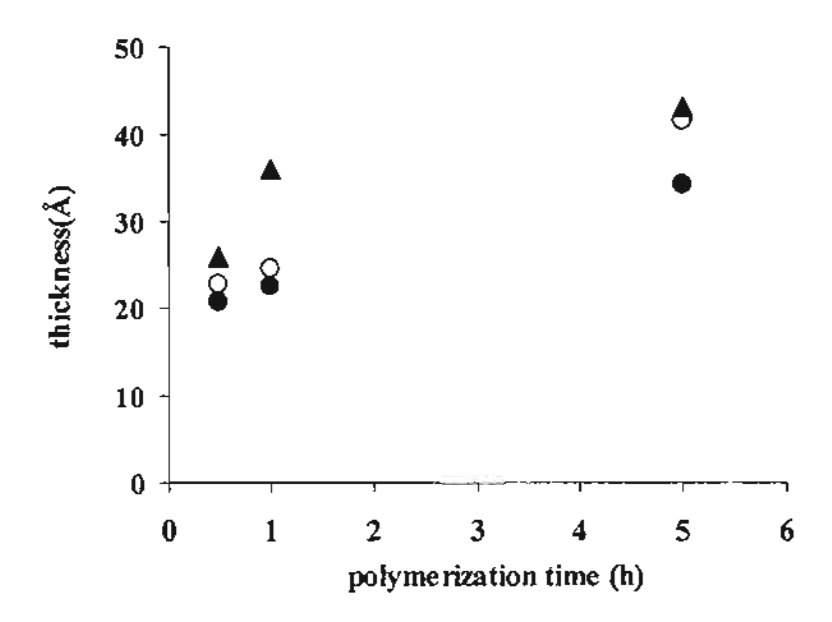


Figure 4.25 Ellipsometric thickness of PMPC brushes grown from silicon-supported mixed tris(TMS)/ $\infty$ -bromoisobutyrate monolayer having 82%tris(TMS) coverage versus polymerization time in methanol :  $n_3$  ( $\bullet$ ),  $n_6$  ( $\bigcirc$ ) and  $n_{10}$  ( $\triangle$ )

# 4.7 Surface Topography of Polymer Brushes

AFM was used to study in detail the surface topography of the grafted PMPC brush on silicon-supported mixed tris(TMS)/α-bromoisobutyrate monolayer. Figure 4.26 shows AFM images for a clean silicon surface, silicon-supported mixed tris(TMS)/silanol monolayers and their corresponding silicon-supported mixed tris(TMS)/α-bromoisobutyrate monolayers having various % tris(TMS) coverage. In comparison to a clean substrate, the modified surface bearing tris(TMS)/silanol monolayer are almost featureless and relatively smooth. Average roughnesses (Ra) of all modified substrates are listed in Table 4.6. Evidently, neither the coverage of tris(TMS) alone nor the coverage of tris(TMS) and α-bromoisobutyrate significantly alter overall surface roughness.